

Fluorine NMR study of proline-rich sequences using fluoroprolines

Davy Sinnaeve^{1,2}, Abir Ben Bouzayene³, Emile Ottoy⁴, Gert-Jan Hofman^{4,5}, Eva Erdmann³,
Bruno Linclau⁵, Ilya Kuprov⁵, José C. Martins⁴, Vladimir Torbeev⁶ and Bruno Kieffer³

5 ¹Univ. Lille, Inserm, Institut Pasteur de Lille, CHU Lille, U1167 – Labex DISTALZ – RID-AGE – Risk Factors and Molecular Determinants of Aging-Related Diseases, F-59000 Lille, France

²CNRS, ERL9002 - Integrative Structural Biology, F-59000 Lille, France

³Departement of Integrative Structural Biology, IGBMC, Université de Strasbourg, INSERM U1258, CNRS UMR7104, 1, rue Laurent Fries, F-67404 Illkirch, France

10 ⁴Department of Organic and Macromolecular Chemistry, Ghent University, Campus Sterre, S4, Krijgslaan 281, B-9000 Gent, Belgium

⁵School of Chemistry, University of Southampton, Southampton SO17 1BJ, United Kingdom

⁶Institut de Science et d'Ingénierie Supramoléculaires (ISIS), International Center for Frontier Research in Chemistry (icFRC), University of Strasbourg,

15 CNRS UMR 7006, F-67000 Strasbourg, France

Correspondence to: B. Kieffer (kieffer@igbmc.fr) and D. Sinnaeve (davy.sinnaeve@univ-lille.fr)

Abstract. Proline homopolymer motifs are found in many proteins; their peculiar conformational and dynamic properties are often directly involved in those proteins' functions. However, the dynamics of proline homopolymers is hard to study by
20 NMR due to lack of amide protons and small chemical shift dispersion. Exploiting the spectroscopic properties of fluorinated prolines opens interesting perspectives to address these issues. Fluorinated prolines are already widely used in protein structure engineering – they introduce conformational and dynamical biases – but their use as ¹⁹F NMR reporters of proline conformation has not yet been explored. In this work, we look at model peptides where C γ -fluorinated prolines with opposite configurations of the chiral C γ centre have been introduced at two positions in distinct polyproline segments. By looking at
25 the effects of swapping these (4*R*)- and (4*S*)-4-fluoroprolines **within** the polyproline segments, we were able to separate the intrinsic conformational properties of the polyproline sequence from the conformational alterations instilled by fluorination. We assess the fluoroproline ¹⁹F relaxation properties, and exploit the latter in elucidating binding kinetics to the SH3 domain.

30

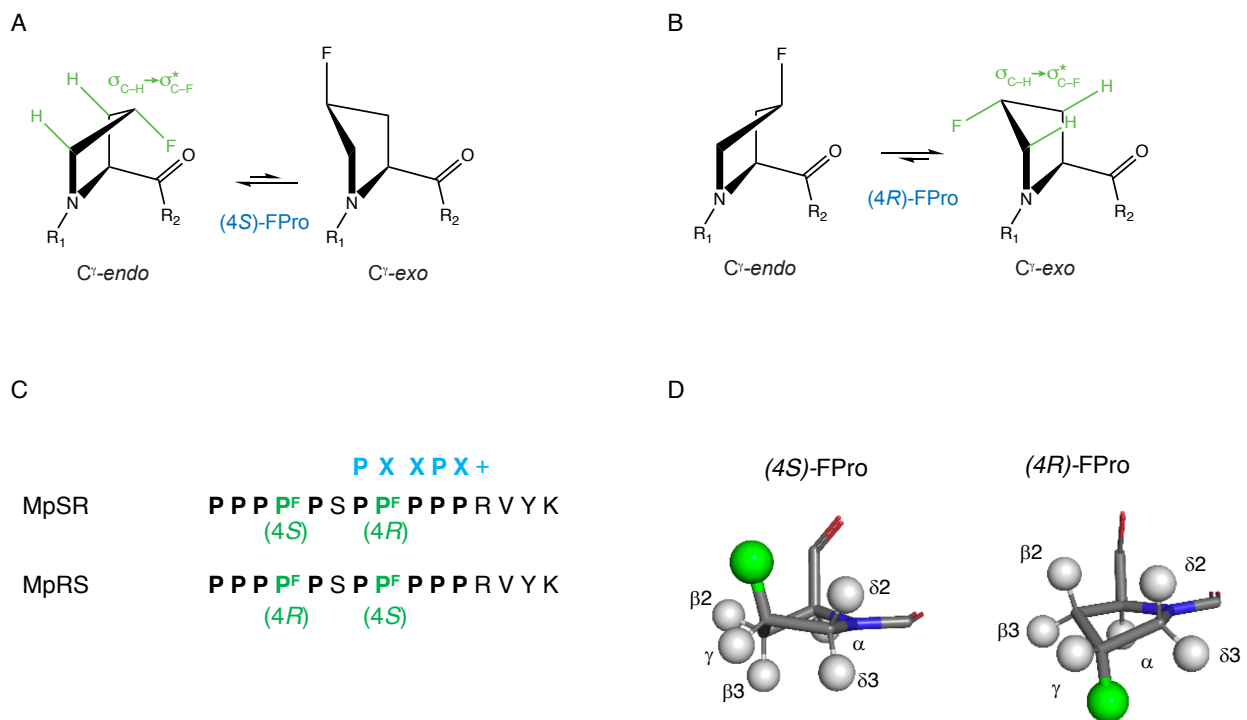
1. Introduction

The use of ^{19}F nuclei in medical and biological magnetic resonance is gaining popularity (Zhang et al., 2017). Since the pioneering incorporation of *p*-fluorophenylalanine (Chaiken et al., 1973) into ribonuclease-S' analogues, dozens of ^{19}F -labelled amino acid analogues have been evaluated (Odar et al., 2015; Mei et al., 2020; Muttenthaler et al., 2021, Salwiczek et al., 2012). Common ways to incorporate fluorinated amino acids in peptides or proteins are: (a) solid phase chemical synthesis (Behrendt et al., 2016); (b) post-translational addition of fluoroalkyl groups to reactive amino acid side chains (Liu et al., 2012); (c) addition of fluorinated precursors, such as fluoroindole, to bacterial culture media prior to protein overexpression (Crowley et al., 2012); (d) using recombinantly expressed orthogonal amber codon tRNA/tRNA synthetase pairs (Sharaf et al., 2015; Gimenez et al., 2021; Gee et al., 2016; Kitevski-LeBlanc et al., 2012). The advantages of ^{19}F nuclei in biological NMR are the absence of background signals, high gyromagnetic ratio, 100% natural abundance, and the sensitivity of ^{19}F chemical shift to the chemical environment (Rastinejad et al., 1995). Fluorine chemical shift range (~50 times wider than that of ^1H) makes it possible to study faster chemical exchange processes than those accessible to ^1H - and ^{13}C -based methods. This is useful in biomolecular interaction studies and examples include the deciphering of the signal transduction pathways through the β 2-adrenergic trans-membrane receptor (Liu et al., 2012), the study of conformer interconversion and allostery that drive the catalytic process in the bacterial enzyme fluoroacetate dehalogenase (Kim et al., 2017), the monitoring of both kinetic and equilibrium thermodynamic binding parameters of a fluorine-labeled Src homology 3 (SH3) protein domain to peptides containing proline-rich motifs (PRM) (Stadmler et al., 2020), and the folding study of a small protein domain (Evanics et al., 2007). A downside of ^{19}F is high chemical shift anisotropy (CSA) – particularly in aromatic rings – resulting in rapid transverse relaxation and broad lines for large biomolecules at high magnetic fields (Kitevski-LeBlanc et al., 2012), although the recently proposed ^{19}F - ^{13}C aromatic TROSY experiment has alleviated this to some extent (Boeszoermyeni et al., 2019).

Fluorination is well known for its significant impact on the properties of organic molecules (Aufiero et al., 2018; Gillis et al., 2015, Berger et al., 2017). Apart from altering the interaction with the solvent (*cf.* hydrophobicity), replacing a hydrogen with fluorine can produce significant structural changes. Firstly, the volume of the moiety increases. Although fluorine is often considered isosteric to hydrogen based on its similar Van der Waals radius ($r_{\text{vdw}}(\text{F}) = 1.47 \text{ \AA}$ vs. $r_{\text{vdw}}(\text{H}) = 1.20 \text{ \AA}$) (Bondi et al., 1964) its covalent radius is significantly larger ($r_{\text{cov}}(\text{F}) = 0.57 \text{ \AA}$ vs. $r_{\text{cov}}(\text{H}) = 0.31 \text{ \AA}$) due to greater C–F bond length (Cordero et al., 2008; O'Hagan et al., 2008). As a result, fluorine may perturb the protein fold when the fluorinated side-chain is tightly packed within a protein structure. Secondly, the polar C–F bond brings in additional charge and polarisability effects (Salwiczek et al., 2012). In aromatic side chains, swapping a single hydrogen for fluorine does not normally (there are exceptions (Salwiczek et al., 2012; Boeszoermyeni et al., 2020; Yoshida et al., 1960)) alter the fold or the function of the protein (Welte et al., 2020). In contrast, fluorinating an aliphatic CH group can radically change local rotamer populations (O'Hagan et al., 2008; O'Hagan et al., 2012). This effect has been put to good use (Salwiczek et al., 2012; Berger et al., 2017), particularly in fluorinated prolines (Kubyshevskiy et al., 2021; Verhoorck et al., 2018; Newberry et al., 2016).

Proline is the only proteinogenic amino acid with a secondary amino group, thus allowing for the *cis*-peptide bond isomer to be significantly populated. In addition, its pyrrolidine ring can adopt either a $\text{C}\gamma$ -*endo* or $\text{C}\gamma$ -*exo* conformation, with a slight preference for the former. Single or double fluorination at the β - and/or γ -positions shifts these conformational equilibria in a stereospecific way. For instance, (4*R*)-fluorination favours the $\text{C}\gamma$ -*exo* ring conformer and enhances the *trans* isomer population, while (4*S*)-fluorination does the opposite (Fig. 1) (Eberhardt et al., 1996; Panasik et al., 1994).

This is caused by stabilizing $C-H\sigma_{(HOMO)} \rightarrow C-F\sigma^*_{(LUMO)}$ hyperconjugative delocalization, which is maximal when the C–H bond is antiperiplanar to the C–F bond, a phenomenon generally known as *gauche effect* (Thiehoff et al., 2017). The increased amount of $C\gamma$ -*exo* conformer in (4*R*)-FPro in turn increases the *trans* isomer population since this is the most favourable configuration for further stabilizing hyperconjugative $n \rightarrow \pi^*$ delocalization between carbonyl groups in successive peptide bond (Newberry et al., 2016). Similarly, the reduced $C\gamma$ -*exo* population as well as the steric impact from the longer C–F bond increases the population of the *cis*-isomer in (4*S*)-FPro. The increase or decrease of $n \rightarrow \pi^*$ hyperconjugation have been used to explain stabilization or destabilization of the polyproline-II (PPII) conformation in all-(4*R*)-fluorinated and all-(4*S*)-fluorinated oligoprolines respectively (Hornig et al., 2006). The ability to control the conformational preference of individual proline residues is central to elucidating the role of proline conformation on the stability, folding, and aggregation of various proteins, such as collagen (Holmgren et al., 1998; Shoulders et al., 2009), β_2 -microglobulin (Torbeev et al., 2015; Torbeev et al., 2013) and tau. (Jiji et al., 2016)



80

Figure 1: $C\gamma$ -*endo* and $C\gamma$ -*exo* puckering of the pyrrolidine ring in (4*S*)- and (4*R*)-fluoroprolines shown respectively in **A** and **B**. The *gauche effect* stabilizes the $C\gamma$ -*endo* conformer of (4*S*)-fluoroproline, whereas the $C\gamma$ -*exo* conformer is favoured in (4*R*)-fluoroproline. **C:** Fluoroprolines incorporated in a proline-rich sequence at two positions 4 and 8 highlighted in green. Two peptides are studied: in MpSR (4*S*)-fluoroproline is inserted at the fourth position and (4*R*)-fluoroproline is inserted at the eighth position. In MpRS, the positions of the (4*R*)- and (4*S*)-fluoroprolines are reversed, placing them in the position fourth and eighth, respectively. The canonical SH3 domain binding motif is shown in blue. **D, left side:** 3D model of (4*S*)-fluoroproline where H γ 2 is substituted by a fluorine atom. The carbonyl group and the fluorine atom point towards the same direction. **D, right side:** 3D model of (4*R*)-fluoroproline where H γ 3 is substituted by a fluorine atom. The carbonyl group and the fluorine atom point towards opposite sides.

90

Surprisingly, despite the well-established use of FPro residues in chemical biology, they have so far found very limited attention as ^{19}F NMR reporters in protein studies, in contrast to aromatic amino acids (Verhoork et al., 2018). In the limited protein or peptide studies that have used ^{19}F NMR, it was mainly used to confirm the local conformational state of the fluoroproline residue (Torbeev et al., 2013, Verhoork et al., 2018). To the best of our knowledge, only one study went further and exploited ^{19}F NMR of a *foldon* domain peptide containing (4*R*)-FPro and (4*S*)-FPro residues to monitor the folding/unfolding process as a function of temperature (Dietz et al., 2015). Yet the potential of FPro residues for advanced biomolecular ^{19}F NMR is clear given the abundance of proline in intrinsically disordered protein sequences, the prominent role of proline-rich regions as sites for protein-protein interaction and post-translational modification, the relatively small CSA of ^{19}F nuclei in prolines (thus, narrow lines), and the challenge of detecting minor *cis* isomers (Theillet et al., 2013). Possible explanations are the unknown ^{19}F NMR properties of these residues, as well as their undesirably strong conformational impact.

With the purpose of filling this gap, we have studied the impact of (4*R*)- and (4*S*)-FPro residues on the structure and dynamics of a polyproline peptide harbouring an SH3 binding motif, and used ^{19}F NMR to investigate the impact of fluorination on the binding affinity. We designed model peptides containing (4*R*)- and (4*S*)- fluorinated prolines with a sequence based on the motif located at the C-terminal part of the retinoic acid hormone nuclear receptor RAR γ that specifically binds to the third SH3 domain of the Vinexin β protein (Lalevee et al., 2010). First, we explored the impact of FPro introduction on the surrounding peptide sequence, and verified the preferred FPro ring pucker within the polyproline context. Next, we used ^{19}F relaxation analysis to gain insights into the local dynamics of the peptide. Finally, we monitored the interaction of the model peptides with the vinexin β SH3 domain using ^{19}F NMR, and demonstrated that FPro conformational bias can be used to modulate the kinetics of protein binding to proline-rich motifs. This work paves the way to using fluoroprolines as ^{19}F NMR reporters in protein interaction studies, where the conformational bias caused by fluorine is exploited to obtain information on binding kinetics.

2. Results

2.1 Assignment and spectral analysis of model peptides

The model peptide sequences shown in Fig. 1C contain two segments of five prolines separated by a single serine, and terminate with a four-residue sequence (RVYK) required for the SH3 class II binding specificity. FPro residues were inserted at positions 4 and 8, which are not directly involved at the protein-peptide interface according to homology models of PPII helices-SH3 complexes (Saksela et al., 2012). Position 4, located in the first polyproline segment, falls outside the expected PXXPX+ binding motif while proline 8, which is located within the canonical SH3-PPII binding motif, is expected to be solvent-exposed (Supplementary Fig.1). Thus, the fluorine atoms are not expected to contribute significantly to the protein-peptide binding interface. Two peptides were considered, with (4*R*)- and (4*S*)-FPro substitutions at positions 4 and 8 (hereafter named MpRS), or introduced at positions 8 and 4 (MpSR).

Full ^1H and ^{13}C chemical shift assignments of the non-proline and FPro residues in D_2O were achieved using standard ^1H - ^1H NOESY, ^1H - ^1H TOCSY and ^1H - ^{13}C HSQC experiments. The 8 non-fluorinated proline residues have very similar chemical shifts, but full assignment could still be achieved using a 2D ^1H - ^{13}C HSQC-NOESY experiment with very high ^{13}C digital resolution (*ca.* 4 Hz, see experimental section) (Fig. 2). For this, the spectral window was set to a narrow ^{13}C chemical shift region of 3 ppm containing the proline $\text{C}\delta$ resonances. To avoid interference from folded ^{13}C - $\text{H}\alpha$ autocorrelation peaks, a gradient-enhanced frequency-selective ^{13}C 180° refocusing pulse was applied in the HSQC experiment. At this spectral resolution, the minute $\text{C}\delta$ chemical shift dispersion (0.3 ppm for prolines 2 to 11 in MpSR) allowed resolving the sequential $\text{H}\delta(i)$ to $\text{H}\alpha(i-1)$ NOE cross-peaks and thus completing ^1H and ^{13}C chemical shift assignment of both peptides (Table 1).

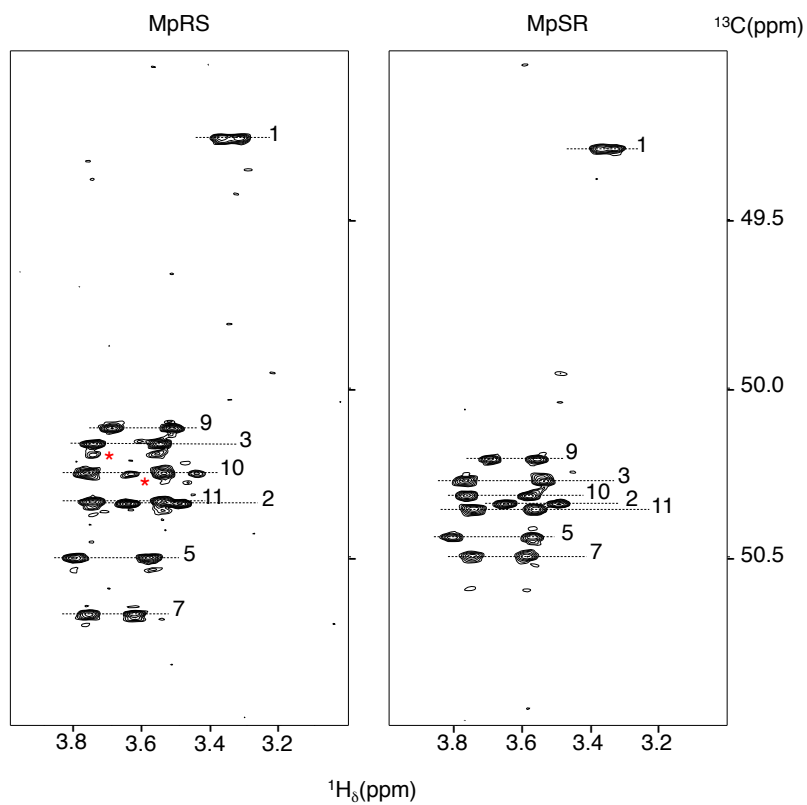


Figure 2: ^1H - ^{13}C HSQC-NOESY (mixing time: 80 ms) with a narrow ^{13}C window focussing on the $^{13}\text{C}_\delta/\text{H}_\delta$ correlations regions of both MpRS and MpSR peptides, recorded at 298 K and 700 MHz. The numbers indicate the position of the residue in the sequence. The red asterisks highlight minor forms of prolines.

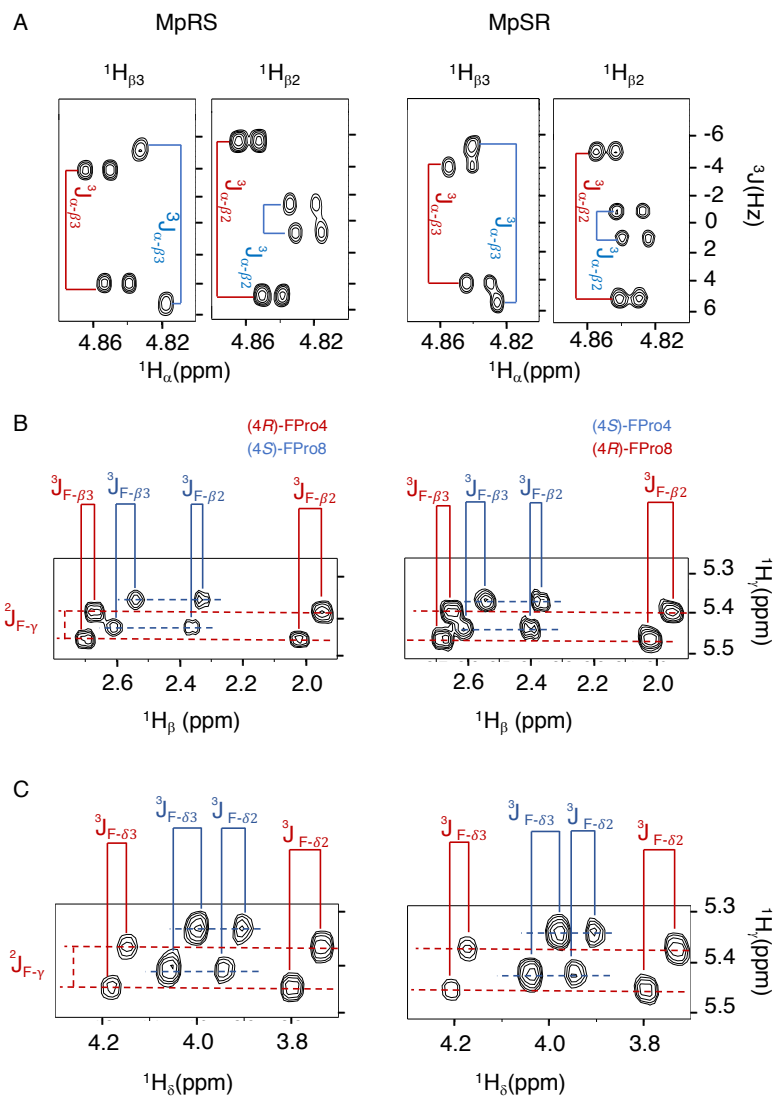
Table 1: Chemical shift assignments of MpRS and MpSR peptides. $\Delta\delta$ is the chemical shift difference between $^{13}\text{C}\beta$ and $^{13}\text{C}\gamma$ resonances used as indicator for *cis* and *trans* conformations of the Xaa-Pro peptide bond. $\Delta\text{C}\alpha$ is the chemical shift difference between the measured $^{13}\text{C}\alpha$ and the corresponding random coil values. Chemical shifts were measured in D_2O at pH 7, 298 K and referenced to DSS-d_6 .

| MpRS | | | | | | | | | | |
|------------------|-----------------------------|----------------------------|-----------------------------|-----------------------------------|-----------------------------|----------------------------|-----------------------------|-----------------------------|----------------------------------|--|
| | Hα | Hβ | Hγ | Hδ | Cα | Cβ | Cγ | Cδ | $\Delta\delta$ | $\Delta\text{C}\alpha$ |
| Pro1 | 4.61 | 2.54 2.04 | 2.04 | 3.42 3.37 | 61.76 | 30.86 | 26.51 | 49.28 | 4.35 | -1.58 |
| Pro2 | 4.76 | 2.39 1.88 | 2.01 | 3.69 3.54 | 61.62 | 30.57 | 27.26 | 50.37 | 3.31 | -1.72 |
| Pro3 | 4.71 | 2.29 1.84 | 2.05 | 3.80 3.60 | 61.24 | 30.49 | 27.32 | 50.20 | 3.17 | -2.10 |
| (4R)-FPro | 4.89 | 2.73 2.03 | 5.44 | 4.20 3.81 | 59.72 | 37.22 | 95.66 | 56.52 | -58.44 | -3.62 |
| Pro5 | 4.45 | 2.28 1.88 | 2.01 | 3.85 3.64 | 62.86 | 32.06 | 27.26 | 50.51 | 4.80 | -0.48 |
| Ser6 | 4.70 | 3.85 3.72 | | | 56.46 | 62.97 | | | | -2.25 |
| Pro7 | 4.62 | 2.37 1.96 | 2.05 | 3.82 3.68 | 61.53 | 30.78 | 27.32 | 50.69 | 3.46 | -1.81 |
| (4S)-FPro | 4.86 | 2.62 2.38 | 5.41 | 4.07 3.96 | 60.35 | 36.90 | 95.63 | 56.50 | -58.73 | -2.99 |
| Pro9 | 4.69 | 2.3 1.87 | 2.02 | 3.74 3.56 | 61.22 | 30.52 | 27.25 | 50.13 | 3.27 | -2.12 |
| Pro10 | 4.68 | 2.31 1.87 | 2.02 | 3.82 3.59 | 61.19 | 30.73 | 27.25 | 50.25 | 3.48 | -2.15 |
| Pro11 | 4.37 | 2.26 1.83 | 2.00 | 3.8 3.59 | 62.82 | 32.01 | 27.26 | 50.33 | 4.75 | -0.52 |
| Arg12 | 4.24 | 1.68 1.67 | 1.54 1.47 | 3.13 3.13 | 55.80 | 30.80 | 26.96 | 43.17 | | -0.98 |
| Val13 | 4.06 | 1.94 | 0.85 0.83 | | 61.83 | 33.03 | 20.97 20.44 | | | -0.71 |
| Tyr14 | 4.57 | 3.01 2.87 | | 7.10 H ϵ 6.78 | 57.51 | 39.09 | | 53.21 C ϵ 37.98 | | -0.67 |
| Lys15 | 4.28 | 1.84 1.72 | 1.34 1.33 | 1.65 1.62 H ϵ 2.92 | 55.16 | 32.72 | 24.63 | 28.84 C ϵ 41.82 | | -1.80 |

MpSR

| | H α | H β | H γ | H δ | C α | C β | C γ | C δ | $\Delta\delta$ | $\Delta C\alpha$ |
|------------------|------------|-----------|------------|-------------------|------------|-----------|------------|--------------------|----------------|------------------|
| Pro1 | 4.61 | 2.54 | 2.05 | 3.42 | 61.75 | 30.91 | 26.52 | 49.3 | 4.39 | -1.59 |
| Pro2 | 4.76 | 2.39 | 2.01 | 3.70 | 61.65 | 30.64 | 27.27 | 50.36 | 3.37 | -1.69 |
| Pro3 | 4.63 | 2.38 | 2.06 | 3.82 | 61.31 | 30.63 | 27.30 | 50.28 | 3.33 | -2.03 |
| (4S)-FPro | 4.87 | 2.59 | 5.42 | 4.07 | 60.32 | 36.97 | 95.09 | 56.55 | -58.12 | -3.02 |
| Pro5 | 4.43 | 2.27 | 2.02 | 3.85 | 63.06 | 31.89 | 27.27 | 50.44 | 4.62 | -0.28 |
| Ser6 | 4.71 | 3.84 | | | 56.24 | 63.04 | | | | -2.47 |
| Pro7 | 4.68 | 2.31 | 2.02 | 3.79 | 61.51 | 30.66 | 27.26 | 50.50 | 3.40 | -1.83 |
| (4R)-FPro | 4.88 | 2.72 | 5.45 | 4.22 | 59.77 | 37.20 | 95.10 | 56.58 | -57.90 | -3.57 |
| Pro9 | 4.71 | 2.32 | 2.03 | 3.75 | 61.37 | 30.68 | 27.29 | 50.21 | 3.39 | -1.97 |
| Pro10 | 4.68 | 2.28 | 1.99 | 3.81 | 61.26 | 30.62 | 27.27 | 50.32 | 3.35 | -2.08 |
| Pro11 | 4.37 | 2.26 | 2.00 | 3.79 | 62.79 | 32.01 | 27.27 | 50.36 | 4.74 | -0.55 |
| Arg12 | 4.23 | 1.70 | 1.56 | 3.13 | 55.82 | 30.82 | 26.94 | 43.17 | | -0.96 |
| Val13 | 4.06 | 1.93 | 0.86 | | 61.82 | 33.04 | 20.41 | | | -0.72 |
| Tyr14 | 4.57 | 3.01 | 0.83 | 7.10 | 57.52 | 39.09 | 20.98 | 53.21 | | -0.66 |
| | | 2.88 | | H ϵ 6.78 | | | | C ϵ 37.98 | | |
| Lys15 | 4.27 | 1.84 | 1.34 | 1.63 | 55.23 | 32.74 | 24.61 | 28.87 | | -1.73 |
| | | | | H ϵ 2.93 | | | | C ϵ 41.82 | | |

When comparing the two peptides, ^1H and ^{13}C chemical shifts of each type of FPro (4R or 4S) turn out nearly identical, independently of their position in the sequence, suggesting that the local conformation of the pyrrolidine ring is not sensitive to the sequence context, but is dictated by the fluorination stereochemistry at the C γ -center. To confirm this, we measured ^1H - ^{19}F and $^1\text{H}\alpha$ - $^1\text{H}\beta$ scalar couplings within the FPro residues (Table 2). Heteronuclear ^1H - ^{19}F couplings were measured in 2D ^1H - ^1H TOCSY spectra using the E.COSY cross-peak pattern $^1\text{H}\gamma$ - $^1\text{H}\beta$ and $^1\text{H}\gamma$ - $^1\text{H}\delta$ correlation peaks, while the homonuclear $^1\text{H}\alpha$ - $^1\text{H}\beta$ couplings were measured using SERF experiments (see experimental section) (Fig. 3). These latter couplings are diagnostic of the ring pucker, and a visual inspection of the coupling patterns observed for MpRS and MpSR peptides immediately indicates that both (4R or 4S) FPro retain their *exo* or *endo* ring pucker in the context of a polyproline segment. These scalar couplings are compared with the literature values determined for the free amino acid (Table 2) (Gerig et al., 1973), and turn out to be very similar, except for the $^3J_{\text{F}-\alpha 2}$ coupling in (4S)-FPro where a difference of about 5 Hz is seen. The reason for this is unclear, but could be due to the presence of either a neighbouring amide or amine group in the peptide or free amino acid, respectively. Thus, it can be concluded that the strong bias of the five-membered ring conformation introduced by 4-monofluorination (Gerig et al., 1973; DeRider et al., 2002) is fully preserved within the oligoproline context. Using density functional theory (M06/cc-pVDZ in SMD water), we previously calculated for Ac-FPro-OMe that the C γ -*exo*:C γ -*endo* population ratios are 93:7 for (4R)-FPro and 1:99 for (4S)-FPro (Hofman et al., 2018; Hofman et al., 2019). For the purpose of NMR conformation and dynamic analysis, it is thus fair to assume that only one ring conformer is present. It is known that proline normally interconverts between the C γ -*exo* and C γ -*endo* ring conformations within oligoprolines while adopting a PPII helix (Hornig et al., 2006; Wilhelm et al., 2014). Similar to the concept of conformational frustration (Ferreiro et al., 2014), it can be stated that proline fluorination creates a form of “dynamic frustration” within the polyproline helix.



165 **Figure 3:** Puckering analysis of fluoroprolines. **A:** Homonuclear coupling constants $^3\text{J}_{\text{H-H}2}$ and $^3\text{J}_{\text{H-H}3}$ of the (4R) (in red) and (4S) (in blue) fluoroprolines in MpSR and MpRS peptides measured from SERF experiments at 298 K. **B:** The $^3\text{J}_{\text{F-H}}$ heteronuclear coupling constants extracted from 2D ^1H - ^1H TOCSY spectra using the E.COSY cross-peak pattern. **C:** The $^3\text{J}_{\text{F-H}}$ heteronuclear coupling constants extracted from 2D ^1H - ^1H TOCSY spectra using the E.COSY cross-peak pattern.

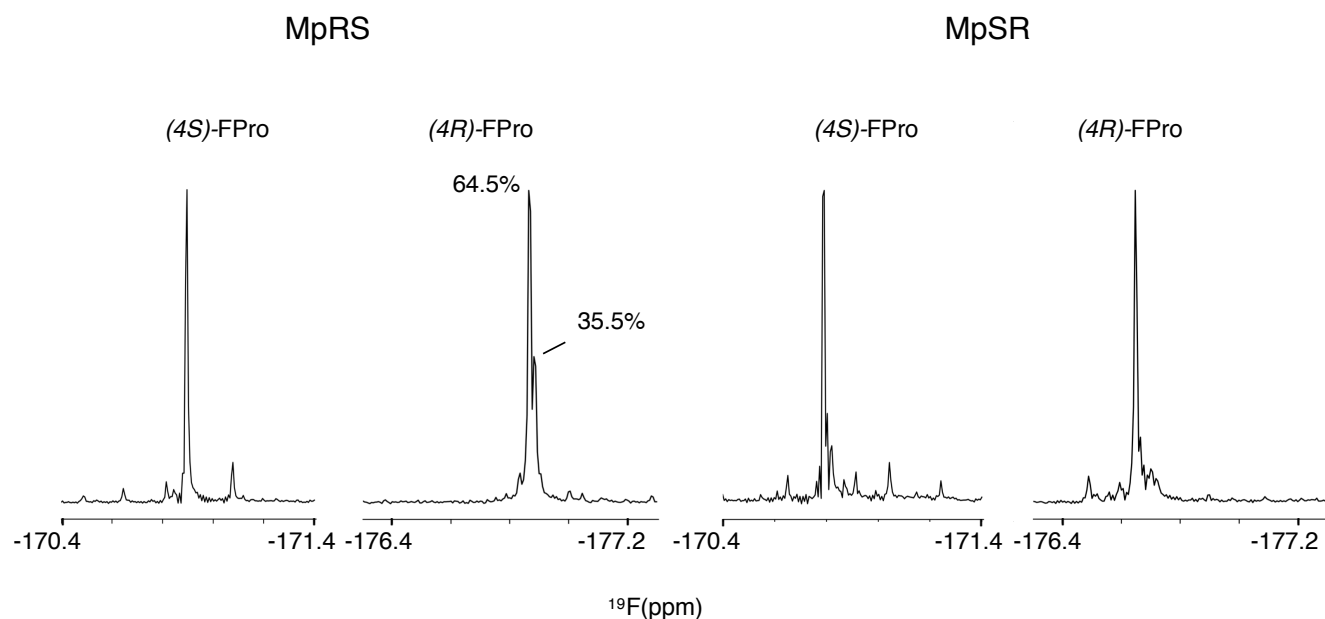
Table 2: Comparison of the scalar coupling constants (in Hz) of (4*R*)-FPro and (4*S*)-FPro measured in MpRS and MpSR peptides with those reported for the free fluoroproline residues (Gerig et al., 1973).

| | MpRS | | MpSR | | Free amino acid | |
|------------------------|------------------|------------------|------------------|------------------|--------------------|--------------------|
| | P4 (4 <i>R</i>) | P8 (4 <i>S</i>) | P4 (4 <i>S</i>) | P8 (4 <i>R</i>) | (4 <i>R</i>)-FPro | (4 <i>S</i>)-FPro |
| $^3J_{F-\beta 2}$ | 42.3 | 21.0 | 20.9 | 42.1 | 40.5 | 20.5 |
| $^3J_{F-\beta 3}$ | 18.8 | 42.5 | 43.1 | 18.9 | 19.6 | 41.9 |
| $^3J_{F-\delta 2}$ | 38.2 | 24.6 | 24.7 | 38.3 | 37.4 | 19.4 |
| $^3J_{F-\delta 3}$ | 21.7 | 35.2 | 35.4 | 21.9 | 20.1 | 37.6 |
| $^3J_{\alpha-\beta 2}$ | 10.1 | 3.0 | 3.1 | 10.2 | 10.4 | 2.8 |
| $^3J_{\alpha-\beta 3}$ | 8.1 | 10.5 | 10.2 | 8.1 | 8.1 | 10.5 |

175 For the non-fluorinated prolines, the ^{13}C chemical shifts are mostly similar in the MpRS and MpSR peptides (Table 1 and Supplementary Fig.2), suggesting that the overall conformational properties of the peptide are not greatly affected by the permutation of the two FPro residues. It is also observed that the insertion of the PPII destabilizing (4*S*)-FPro within both polyproline segments does not alter the intensities of the strong $\text{H}\alpha(i-1)$ to $\text{H}\delta(i)$ NOE cross-peaks observed between all prolines of the segment including the (4*S*)-FPro. In addition, the chemical shift differences between $^{13}\text{C}\beta$ and $^{13}\text{C}\gamma$ are found
 180 within 5 ppm for all eight natural prolines, indicating a *trans* conformation of the Xaa-Pro peptide bond (Table 1) (Schubert et al., 2002). The dynamics of the non-fluorinated prolines are also not impacted by the insertion of either (4*S*)- or (4*R*)-FPro, as measured from the difference between the diastereotopic $\text{H}\delta$ chemical shifts (Ahuja et al., 2016) (Supplementary Fig.3). All of this indicates that the overall PPII secondary structure of a polyproline segment is maintained, regardless of the conformational bias of the individual fluoroproline residue. Nevertheless, subtle ^{13}C chemical shift differences between both
 185 peptides are observed in the prolines neighboring the FPro residues (3, 5, 7 and 9) (Table 1 and Supplementary Fig.2), with the most pronounced differences seen in the $\text{C}\delta$ chemical shifts (Fig. 3). Indeed, it has been shown for Ac-FPro-OMe model compounds that the (4*R*)- and especially the (4*S*)-FPro residues change the preferred ψ dihedral angle (DeRider et al., 2002). The FPro residues thus appear to cause small local conformational equilibrium or dynamics changes in the local PPII helix backbone, and further detailed conformational analysis is ongoing to confirm and quantify this effect. Finally, a minor set of
 190 peaks for prolines 10 and 3 is observed in the MpRS peptide in the 2D ^1H - ^{13}C HSQC-NOESY spectrum (Fig. 2); their origin could not be established.

The ^{19}F NMR spectra of each peptide are shown in Fig. 4. The assignment of the ^{19}F resonances can be made by comparing their chemical shifts with those of the Ac-FPro-OMe model compounds (*ca.* -178 ppm for (4*R*)-FPro, -173 ppm for (4*S*)-FPro) (Hofman et al., 2019). Just as for ^1H and ^{13}C chemical shifts, ^{19}F chemical shifts of each type of FPro change only
 195 slightly between peptides. Several smaller peaks are found near the main peak of the (4*R*)-FPro at position 4 of the MpRS peptide, with one accounting for 35% of the total signal integral. By analyzing this particular sample by analytical HPLC and mass-spectrometry we identified this species as an impurity (with mass increase of 14 Da that is localized to Pro1 residue based on tandem MS^2 experiment). Other minor peaks can correspond to minor forms of the peptide where a single proline or fluoroproline is in the *cis*-form. For oligoproline sequences, the *cis* form of internal prolines are known to be typically
 200 populated at a few percent, while the N- and C-terminal prolines can have populations above 10% (Best et al., 2007; Urbanek et al., 2020). This illustrates the remarkable sensitivity of fluorine to its chemical environment, as it is able to resolve

not just local conformation of the FPro residue itself, but also chemical modification or conformations of nearby proline residues within the oligoproline.



205 **Figure 4:** 1D ^{19}F NMR spectra showing the fluoroproline signals of the two model peptides MpRS on the left and MpSR on the right. The spectra were recorded at 298 K and 600 MHz in pure D_2O . The (4R)-FPro within MpRS resonance displays a second major species accounting for 35.5% of the total peak integral corresponding to a Hydrolytic and/or oxidative modification of the Pro1.

210 2.2 ^{19}F relaxation and dynamics

Spin relaxation rates are a useful source of information on molecular structure and dynamics. However, ^{19}F relaxation theory is rather complex, with multiple dipole-dipole (DD) interactions to neighboring protons, strong chemical shift anisotropy (CSA), and a multitude of cross-correlations (Dalvit et al., 2017; Lu et al., 2019). This stands in contrast with protein backbone ^{15}N relaxation where the dominant DD interaction with a single proton and ^{15}N CSA is well understood. A quantitative analysis of ^{19}F relaxation rates for both the (4R)- and (4S)-FPro residues in terms of dynamics thus requires knowledge of the various ^1H - ^{19}F distances within the fluoroproline structure, and also of the ^{19}F CSA tensor. These were obtained (Table 3) using density functional theory for the energy minimum structures of C_γ -*exo* and C_γ -*endo* ring conformations in the *trans* form of N-acetyl-FPro-NMe₂, where the capping groups were chosen to emulate the oligoproline peptide context. In each case, multiple protons had sufficiently small distances to the ^{19}F nucleus in order to significantly contribute to DD relaxation. While the distance to the H_γ proton remains constant (2.0 Å), the distances to H_β and H_δ protons change with conformation (Table 3) (Gerig et al., 1973). Proline ring conformation also has a profound effect on the anisotropy parameter $\Delta\sigma$ of the chemical shift tensor: the major conformers (C_γ -*exo* for 4R-FPro and C_γ -*endo* for 4S-FPro) have $\Delta\sigma \approx -80$ ppm, while the minor conformers have $\Delta\sigma \approx -30$ ppm.

It has been shown that the proline ring pucker exchange occurs on a picosecond time scale (London et al., 1978; Sarkar et al., 1986; Kang et al., 2007), and thus faster than the overall tumbling of a peptide. Fluorine relaxation rates will be sensitive to this internal motion. However, because DD and CSA interactions vary in a correlated way with this motion, standard

rotational diffusion autocorrelation functions cannot be used. Fortunately, as shown in the previous section, within the polyproline context both FPro residues adopt one dominant conformation. Although the work reported here can proceed, it would be beneficial in the long run to design case-specific relaxation models that involve a picosecond scale correlated switch in the spin Hamiltonian parameters.

Theoretical calculations of all relaxation rates were performed using the brute-force numerical implementation of Bloch-Redfield-Wangsness relaxation theory available in *Spinach 2.6*, which automatically accounts for all dipole-dipole interactions, all chemical shift anisotropies, and all of their cross-correlations (Hogben et al., 2011). Molecular geometries and the relevant magnetic parameters (chemical shielding tensors and J -couplings) were imported from DFT calculations. The molecules in question are small enough that no spin system truncation is necessary. Longitudinal ^{19}F relaxation rates were calculated for rotational correlation times between 10 ps and 100 ns at 14.1 Tesla (Fig. 5A), for both *exo* and *endo* conformers to evaluate the impact of proline ring pucker. The correlation time dependence of longitudinal relaxation rates for the major conformers of all FPro residues shows a peculiar ‘camel hump’ shaped profile, with two maxima at 0.3 ns and at 4.4 ns. The same picture was reported earlier for fluorinated aromatic amino acids based on a simplified relaxation model (Dalvit et al., 2017). It is caused by CSA and dipolar ^1H - ^{19}F relaxation contributions being maximal at different frequencies, namely the fluorine Larmor frequency (ω_{F}) and the difference between proton and fluorine Larmor frequencies ($\omega_{\text{H}} - \omega_{\text{F}}$), respectively. For the minor conformers, the maximum at 0.3 ns is much lower than the one at 4.4 ns due to the lower CSA (Table 3). This demonstrates that, for longitudinal ^{19}F relaxation, the contribution of motions operating at time scales up to about 3 ns are strongly influenced by the ring pucker distribution. When assuming only the major ring pucker to be present – as in the polyproline context – R_1 shows very little contrast in the 0.1 ns to 10 ns range, implying it is not an appropriate parameter to unambiguously probe dynamics. The experimental relaxation rates measured for MpRS and MpSR peptides at 298K are reported in Table 4; they fall into a narrow range between 2.1 and 2.3 s^{-1} , in agreement with the calculated values within the aforementioned correlation time range.

Transverse ^{19}F relaxation rates (measured using the CPMG sequence with a half-echo delay of 200 μs) show the usual monotonic increase with the rotational correlation time (Fig. 5B). The difference in CSA between *exo* and *endo* puckers has a clear impact throughout, thereby complicating its interpretation in situations where puckers would be exchanging. To assess the contribution of slow motions, transverse relaxation rates were also measured using a spin echo (Table 4). This revealed about double values throughout, revealing exchange contributions on the ms time scale at both sites for both MpRS and MpSR peptides. As residual exchange contributions cannot be excluded in the CPMG experiment, an interpretation of transverse relaxation rates would also be unreliable. The origin of the exchange contribution is unclear, but possibly may arise from transient interactions between the polyproline segment and the flanking sequence (RVYK). Further studies will be required to investigate this unexpected finding.

In contrast to R_1 and R_2 , ^1H - ^{19}F cross-relaxation rates within the same carbon centre are purely dipolar and therefore likely to be easier to analyse. The $^1\text{H}_{\gamma}$ - ^{19}F NOE is ideal because H_{γ} has a distinct chemical shift at 5.6 ppm, allowing selective RF irradiation without perturbing the remaining protons of the proline ring; $^1\text{H}_{\gamma}$ - ^{19}F distance is independent on ring pucker. Fig. 5C shows the calculated steady-state ^{19}F NOE upon $^1\text{H}_{\gamma}$ saturation as a function of rotational correlation time. Just as for the R_1 curves, at long correlation times nearly identical curves for both the (4R)- and (4S)-FPro residues in each pucker are found, while at short correlation times a small difference is found between the puckers due to the dissimilar CSA. Importantly, the sigmoidal transition parts between fast-motion and slow-motion limits are similar in all four cases, making $^1\text{H}_{\gamma}$ - ^{19}F NOE a reliable parameter sensitive to motions with correlation times between 0.1 and 4 ns.

Experimentally, $^{19}\text{F}_{\gamma}$ signal intensities were measured for several H_{γ} selective irradiation times, leading to the observation of NOE build-up curves that were fitted with a single exponential function to extract the cross-relaxation rates (Fig. 5D-E). For both peptides, the steady-state NOE ranges from -6.8 % at position 4 to -19.9 % at position 8 (Table 4), indicating faster

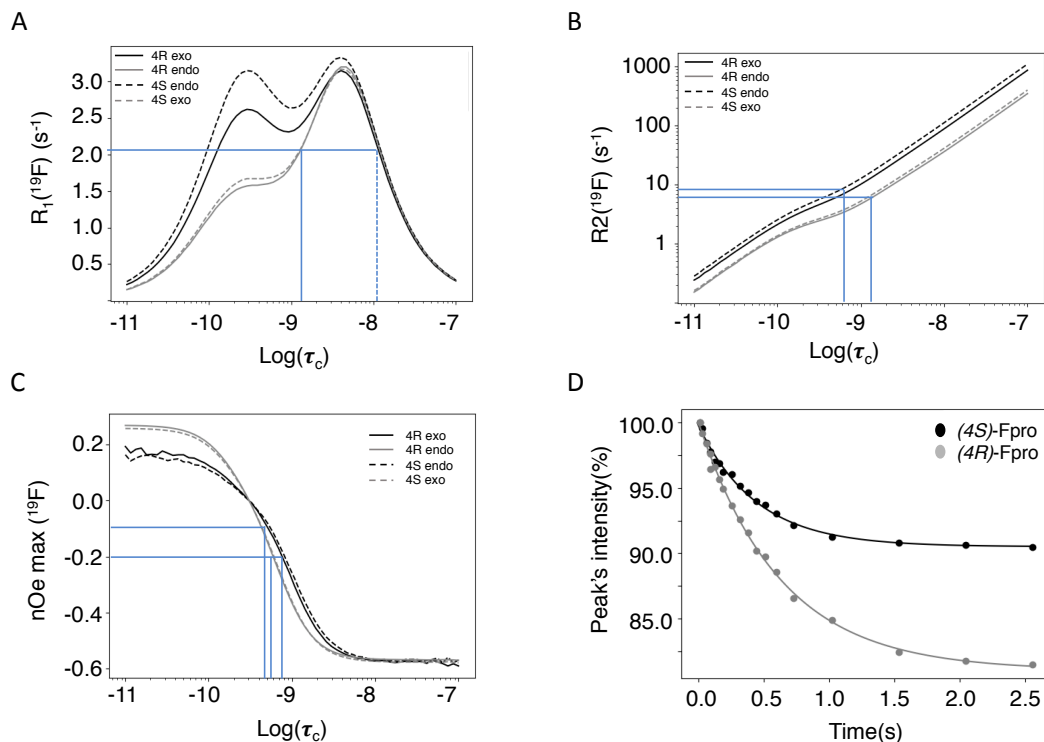
dynamics experienced by the first polyproline segment compared to the second. These values correspond to rotational correlation time estimates of 0.5 ns for the proline at position 4, and 0.8 ns for the proline at position 8. These correlation times suggest that local motions are different for the two polyproline segments, irrespective of the identity of the FPro residue. The reason for this difference between both polyproline segments is not obvious, and further relaxation or conformational studies will be required. We speculate that the distinct flanking sequences of each polyproline segment may determine their overall conformational and dynamical behavior, in a similar way as has recently been shown for other homopolymer sequences such as polyglutamine (Eftekharzadeh et al., 2016, Urbanek et al., 2020).

Table 3: Internuclear distances between ^{19}F atom and the neighboring protons for representative conformers of major and minor conformations of the (4*R*)- and (4*S*)- FPro and corresponding ^{19}F CSA tensor parameters derived from Gaussian calculations. $\Delta\delta$ is the chemical shift tensor anisotropy, η is the asymmetry parameter, and δ_{xy}^{anti} , δ_{xz}^{anti} , δ_{yz}^{anti} are the antisymmetric components to the full CSA tensor in the principal axes coordinate system of the symmetric part of the tensor.

| | Distances (Å) | | | | | ^{19}F CSA tensor | | | | |
|-----------------------------|---------------|---------------|---------------|----------------|----------------|----------------------------|--------|-------------------------------|-------------------------------|-------------------------------|
| | F-H γ | F-H β_2 | F-H β_3 | F-H δ_2 | F-H δ_3 | $\Delta\delta$ (ppm) | η | δ_{xy}^{anti} (ppm) | δ_{xz}^{anti} (ppm) | δ_{yz}^{anti} (ppm) |
| (4 <i>R</i>)-exo major | 2.03 | 3.29 | 2.56 | 3.3 | 2.5 | -74.2 | 0.120 | 4.71 | 2.21 | -3.45 |
| (4 <i>R</i>)-endo minor | 2.02 | 2.89 | 2.50 | 2.97 | 2.44 | -25.6 | 0.396 | 7.29 | 2.34 | 4.42 |
| (4 <i>S</i>)-endo major | 2.01 | 2.49 | 3.29 | 2.4 | 3.25 | -84.9 | 0.392 | -3.26 | -4.27 | -6.01 |
| (4 <i>S</i>)-exo minor | 2.02 | 2.49 | 2.89 | 2.52 | 2.88 | -33.3 | 0.483 | 5.78 | 2.20 | -2.32 |

Table 4: Experimental longitudinal and transverse relaxation rates together with the nuclear Overhauser effect measured for both peptides at 298 K on a 600 MHz spectrometer.

| | MpRS | | MpSR | |
|--------------------------------|-----------------|-----------------|-----------------|-----------------|
| | P4(4 <i>R</i>) | P8(4 <i>S</i>) | P4(4 <i>S</i>) | P8(4 <i>R</i>) |
| $R_1(\text{s}^{-1})$ | 2.23 ± 0.04 | 2.2 ± 0.01 | 2.30 ± 0.01 | 2.13 ± 0.01 |
| NOE max (%) | -6.8 | -19.9 | -9.3 | -19.0 |
| $\rho(\text{s}^{-1})$ | 1.85 | 1.76 | 2.25 | 1.59 |
| $\sigma(\text{s}^{-1})$ | -0.12 | -0.33 | -0.2 | -0.28 |
| $R_2(\text{s}^{-1})$ Spin Echo | 20.3 ± 0.5 | 24.96 ± 0.6 | 12.4 ± 0.5 | 18.5 ± 0.4 |
| $R_2(\text{s}^{-1})$ CPMG | 8.6 ± 0.5 | 8.2 ± 0.3 | 5.4 ± 0.3 | 9.7 ± 0.5 |



290

Figure 5: **A:** Calculated ^{19}F longitudinal relaxation rates as functions of rotational correlation time. The lines indicate the range of experimental values and their corresponding correlation times. The dotted line indicates a second, unrealistic correlation time for the observed R_1 . **B:** Calculated ^{19}F transverse relaxation rates as functions of rotational correlation time. The lines indicate the range of experimental values and their corresponding correlation times. **C:** Calculated steady state fluorine-proton heteronuclear NOEs. Relaxation data were calculated for (4R)-FPro in the major $C\gamma$ -exo (black plain line) and minor $C\gamma$ -endo (grey plain line) and for (4S)-FPro for the major $C\gamma$ -endo (black dashed line) and the minor $C\gamma$ -exo (grey dashed line) conformations. The lines indicate the range of experimental NOEs and their corresponding correlation times. **D:** Experimental NOE build-up at $F\gamma$ upon selective saturation of $H\gamma$ proton measured for the MpSR peptide at 298 K. The dots are the experimental peak intensities and the solid line is the corresponding fit to a monoexponential function.

295

300

2.3 Impact of proline modifications on the binding of SH3

SH3 domains are small modular protein domains of 50-70 amino acids that typically interact with proline rich motifs (PRM) and that are highly represented in the human genome (Saksela et al., 2012). Many experimental and theoretical studies have been conducted to decipher the molecular mechanisms underlying both binding affinity (in the 0.1-100 μM range of dissociation equilibrium constant K_d) and specificity of SH3 domains that primarily recognize PXXP sequence motifs. This mechanism involves the aromatic indole ring of the tryptophan 37 residue exposed at the surface of the SH3 domain that mediates $\text{CH}\cdots\pi$ interaction with proline residues. Additional binding energy is provided by electrostatic interactions between the SH3 surface residues and those flanking the PXXP motif of the binding partner.

305

In order to measure the binding affinities between the Vinexin β SH3.3 domain and the model peptides, a titration experiment was performed where increasing amounts of peptide were added to a solution of ^{15}N labeled SH3 domain. Apart from MpRS and MpSR peptides, a titration was also performed with a non-fluorinated reference peptide. Just as for most SH3-PRM interaction studies, a gradual frequency shift of a subset of ^1H - ^{15}N correlation peaks in the ^1H - ^{15}N HSQC spectra was observed, indicative of fast exchange between bound and free states of the protein (Fig. 6A). Under this exchange regime,

310

the chemical shifts provide an accurate measure of the bound protein fraction, enabling the determination of an equilibrium dissociation constant K_d (*vide infra*). Interestingly, a striking difference between the peptides is observed in the ^1H - ^{15}N HSQC during the titration, where the trajectory of the tryptophan 37 $^{15}\text{N}_e$ - $^1\text{H}_e$ correlation appears different for the MpRS peptide compared to the MpSR peptide (insert Fig.6). Whether this reflects a direct interaction between the Trp37 aromatic ring with (4S)-FPro8 in the PXXP binding motif, or an alteration of the binding complex indirectly caused by the (4S)-FPro8 residue in MpRS will require further investigation.

320

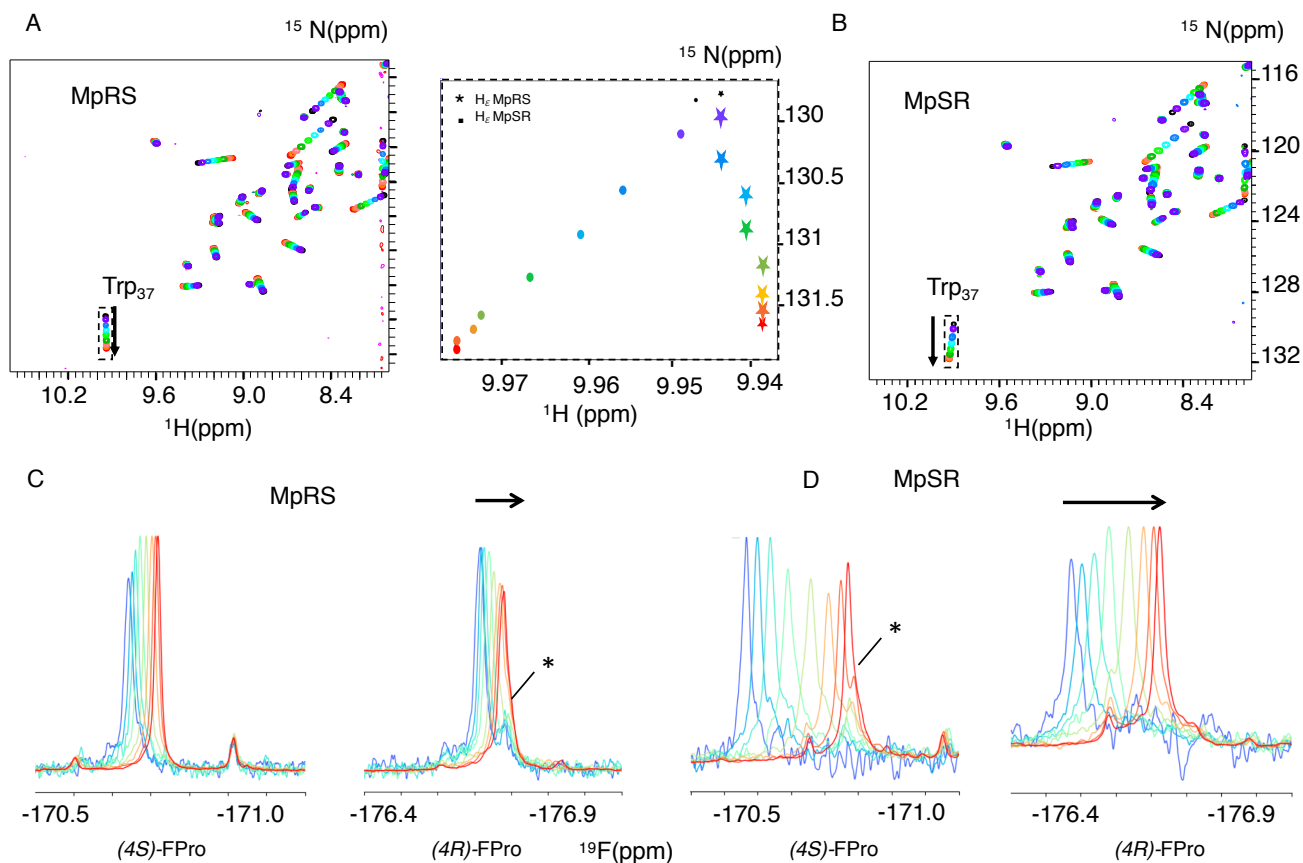


Figure 6: **A** and **B:** A series of ^1H - ^{15}N HSQC spectra of Vinexin β SH3.3 domain recorded upon successive addition of MpRS (**A**) and MpSR (**B**) peptides. The black spectrum corresponds to the first titration point where no peptide is added while the red spectrum corresponds to the last titration point. The arrows indicate the tryptophan 37 N_e - H_e cross-peak trajectories during the titration. The insert in the middle displays a zoom on these cross-peak trajectories shown as the position of the peak center for both MpRS (stars) and MpSR (disks) peptides. **C** and **D:** Series of 1D ^{19}F spectra recorded during the same titration experiment of Vinexin β SH3.3 domain by MpRS (**C**) and MpSR (**D**) peptides. **Peak intensities were normalized to account for the difference in peptide concentrations and number of scans used to record the spectrum.** For the (4R)-FPro4 in MpRS and (4S)-FPro4 in MpSR, a minor peak that overlaps with the main peak at high peptide concentrations is indicated by an asterisk. At low peptide concentrations (blue) the spectra are indicative of a mostly bound form while at high peptide concentrations (red), the spectra converge to those observed for the free peptides.

For the MpRS and MpSR peptides, the peptide-protein titration can also be observed using ^{19}F NMR, allowing to simultaneously monitor the binding event from the perspective of the protein (receptor) and the peptide (the ligand) (Fig. 6C-D). Thanks to the availability of a cryogenic fluorine probehead, the ^{19}F signals could be detected even at the first titration point where the peptide concentration was just 50 μM and **significant broadening was present**. Just like for the ^1H - ^{15}N chemical

shifts, increasing the peptide concentration resulted in a gradual shift of the ^{19}F resonances, indicative of a fast exchange regime. Interestingly, for both the signals from (4*R*)-FPro4 in MpRS and (4*S*)-FPro4 in MpSR, a minor peak is observed that does not shift during the titration (highlighted by a star in Fig. 6C and 6D). This minor peak thus appears to belong to a state that is not competent for SH3 binding. This proline is located in the first polyproline segment and this observation implies that at least two states of the complex are evidenced by the fluorine resonance at this position. At higher peptide concentrations, the peaks sharpen up with addition of peptide, which can be explained by the increasing fraction of the unbound peptide and thus lower amount of exchange broadening and faster tumbling correlation time. Visual inspection of the ^{19}F spectra reveals that the extent of chemical shift perturbation for both ^{19}F signals in each peptide appears similar, even though P8 falls within the binding motif and P4 outside (Supplementary Fig 1). These comparable CSP may be either due to a specific geometry of the two polyproline segments induced by the serine residue that may bend the PPII helix positioning P4 close to the SH3 surface and/or a dynamic averaging of CSP values due to one-dimensional diffusion of the SH3 domain on the peptide. When comparing the MpRS and MpSR peptides, it can be seen that the extent of chemical shift perturbations is the highest for the MpSR peptide, qualitatively already indicating the higher affinity of MpSR relative to MpRS.

Both the $^1\text{H}/^{15}\text{N}$ chemical shift perturbations of the SH3 domain as well as the ^{19}F chemical shift perturbations of the peptides can be used to assess the binding affinity. For this, the stoichiometry of the binding was first evaluated. Indeed, even though a single canonical PXXPX+ motif is present in the peptide sequence imposing binding specificity, a closer inspection shows that multiple non-specific PXXP motifs can be identified (Fig. 1), potentially leading to additional ways for the SH3 domain binding. For this, two binding models were used where the peptide and SH3 domain can bind either up to a 1:2 ratio or only in a 1:1 ratio. Both the ^{19}F and $^1\text{H}/^{15}\text{N}$ chemical shift data were fitted simultaneously using these models. Based on the goodness of fit reported as the reduced χ^2 , the ternary complex turned out to be unnecessary to explain the data, thus implying that only one SH3 binds to the peptide. The dissociation constants (K_d) found in this way were $96 \pm 30 \mu\text{M}$ for MpSR and $273 \pm 30 \mu\text{M}$ for MpRS. These values are slightly above the values found when only the $^1\text{H}/^{15}\text{N}$ chemical shifts are considered ($75 \mu\text{M}$ and $220 \mu\text{M}$, supplementary table 1) but are within the reported uncertainties that account for the uncertainty on protein and peptides concentration measurements that was estimated to be 15%. However, a strikingly good agreement was observed between the experimental and back-calculated ^{19}F chemical shifts, with a standard deviation of only 1.6 Hz despite the large peak widths of 10-20Hz (Fig. 7A). This excellent precision thanks to the sparsity of the 1D spectrum highlights one important feature of ^{19}F NMR spectroscopy to study molecular interactions. The fitted differences in bound and unbound ^{19}F frequencies is about twice as high for MpSR ($265 \pm 8 \text{ Hz}$ for (4*S*)-FPro4 and $218 \pm 8 \text{ Hz}$ for (4*R*)-FPro8) than for MpRS ($88 \pm 17 \text{ Hz}$ for (4*S*)-FPro4 and $100 \pm 17 \text{ Hz}$ for (4*R*)-FPro8).

In addition, the K_d value was also determined for the non-fluorinated peptide using the $^1\text{H}/^{15}\text{N}$ chemical shift perturbations alone using a binding model with 1:1 stoichiometry, which was found to be $74 \pm 25 \mu\text{M}$, which is similar to the MpSR peptide. It thus appears that the presence of (4*R*)-FPro within the binding motif has a negligible effect on the interaction with SH3, while (4*S*)-FPro significantly lowers the binding affinity despite our observations that suggest a preserved PPII conformation.

The exchange line broadening during the titration experiment also reports on the binding kinetic. Thus, the major ^{19}F peaks were fitted using a Lorentzian line shape and the line widths obtained in this way provide an estimate of the apparent transverse relaxation constant R_2^\ddagger as a function of peptide concentration (Fig. 7B and C), that can be used to derive the binding kinetics. A simplified expression of the exchange contribution to R_2^\ddagger as a function of peptide and SH3 concentration was used that is valid for the fast exchange approximation ($k_{exc} \gg \Delta\omega$) (Kovrigin et al., 2012):

$$R_2^\ddagger = p_f R_2^f + p_b R_2^b + p_f p_b \frac{\Delta\omega^2}{k_{exc}} \quad (1)$$

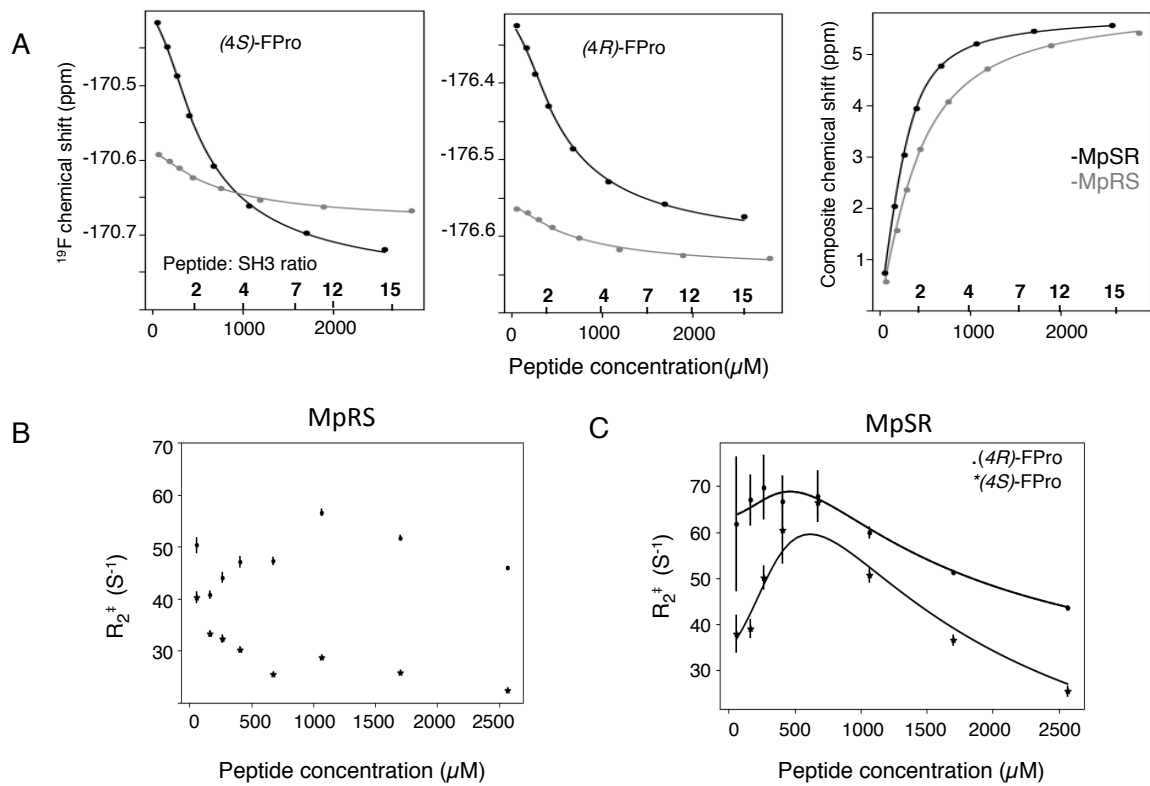
with:

$$k_{exc} = k_{on}([SH3]_{free} + K_d) \quad (2)$$

380

where p_b and p_f are the bound and free fractions of the peptide, R_2^b and R_2^f are the transverse relaxation rates of the bound and the free forms, and $\Delta\omega$ the frequency difference between the bound and free states multiplied by 2π . Taking the values of $\Delta\omega$, p_b , p_f , $[SH3]_{free}$ and K_d from the chemical shift perturbation fitting, the R_2^b , R_2^f and k_{on} values were subsequently fitted to the experimental R_2^\ddagger values. For the MpSR peptide, the optimization was performed independently for the (4S)- and (4R)-FPro ^{19}F signals, leading to a fairly good agreement between experimental and modeled values (Fig. 7B). This provided fitted association kinetic constants k_{on} of $0.9 \cdot 10^8 \pm 0.2 \cdot 10^8 \text{ M}^{-1}\text{s}^{-1}$ and $1.2 \cdot 10^8 \pm 0.2 \cdot 10^8 \text{ M}^{-1}\text{s}^{-1}$ for the (4S)-FPro4 and (4R)-FPro8 signals, respectively. These values are consistent with a simple one-to-one association mechanism driven by a free diffusion process of the two binding partners.

385



390 **Figure 7: A:** ^{19}F chemical shift variation of (4S)-FPro (left) and (4R)-FPro (middle) in MpSR (in black) and MpRS (in gray) peptides extracted from 1D ^{19}F spectra as a function of the total peptide concentrations. The peptide/protein ratios are indicated on the top of the axis. Left panel displays the ^1H , ^{15}N composite chemical shift from ^1H - ^{15}N HSQC. The experimental data (dots) were fitted simultaneously to derive the equilibrium dissociation constants for the two peptides (solid lines). **B:** Variation of the apparent ^{19}F transverse relaxation rates (R_2^\ddagger) as a function of MpRS peptide concentrations. **C:** Variation of the apparent ^{19}F transverse relaxation rates (R_2^\ddagger) derived from the ^{19}F line widths as a function of MpSR peptide concentrations. The black solid lines indicate the expected variation resulting from the fit of the experimental rates with equation 1 and 2 using the transverse relaxation rates of the bound and free peptides (R_2^b , R_2^f) and the on-rate kinetic k_{on} as adjustable parameters.

395

400 | For the MpRS peptide, the profile of R_2^\ddagger as a function of peptide concentration showed a markedly different behavior. After an initial sharpening of about 10 Hz for both ^{19}F signals upon addition of the second peptide aliquot to the SH3 sample, a line broadening was observed for (4*R*)-FPro at position 4 while a continuous sharpening is experienced by the fluorine resonance of (4*S*)-FPro at position 8. This observation is peculiar, as in a simple one-binding site model one would expect a similar profile for both signals. This suggests a more complex binding mechanism involving at least one supplementary
405 | minor state. This is consistent with the observed significant reduction of the chemical shift differences between the bound and free forms of the MpRS peptide compared to MpSR as noted previously. For the MpRS peptide, the combined analysis of fluorine and proton spectral properties is insufficient to specify a specific binding model. However, together with the slight difference observed for the trajectory of the tryptophan $^{15}\text{N}_\epsilon$ - $^1\text{H}_\epsilon$ correlations in the ^1H - ^{15}N HSQC (Fig. 6A), this indicates that the structure or dynamics of the complex are altered by the insertion of (4*S*)-FPro within the canonical SH3 binding motif.
410 |

3. Discussion

(4*R*)- and (4*S*)-fluorinated prolines have, so far, been used in structural biology studies. This work demonstrates their hitherto neglected potential in biomolecular ^{19}F NMR investigations. In contrast to fluorination of most amino acids used in such
415 | studies, proline fluorination changes its conformational and dynamic properties, leading to modified protein-protein interactions. Although this may seem undesirable at first, this can be put to good use – as shown above – to modulate the interaction between a PRM and an SH3 domain. Using a model peptide containing two oligoproline sequences, permutations of two types FPro residues in conjunction with ^{19}F NMR analysis allowed studying the consequences of the conformational biases on the binding equilibrium with the SH3 domain. While the binding affinity appears unaltered by the introduction of (4*R*)-
420 | FPro at position 8 that lies within the SH3 binding motif, the insertion of (4*S*)-FPro at the same position leads to a substantial decrease of the binding affinity. Similar conclusions were drawn in studies involving SH3 domains of cortactin and human hematopoietic-lineage cell-specific protein 1, where insertions of (4*R*)- or (4*S*)-FPro residues in the cognate PRM weakened the binding affinity (Ruzza et al., 2006; Borgogno et al., 2013). Interestingly, these and other (Horng et al., 2006) studies used circular dichroism spectroscopy to confirm that PPII conformational preference is stabilized by (4*R*)-FPro, meaning
425 | that the expected associated increase in SH3 binding affinity is negated by other effects introduced by the presence of the fluorine. Ruzza *et al* (Ruzza et al., 2006; Borgogno et al., 2013) suggested this could be due to a destabilization of the hydrogen bond formed by the proline's carbonyl group due to the inductive effect of fluorine, or by destabilization of proline's interaction with aromatic side-chains of the SH3. Further studies are required to disentangle these effects.

Apart from binding affinities, ^{19}F line shape analysis allowed kinetic information to be extracted. Thanks to the exquisite
430 | susceptibility of the ^{19}F signal line width to chemical exchange phenomena, it was found that the binding on-rate of the SH3 domain is fast and diffusion-limited. This result is consistent with a recent study reporting diffusion limited binding kinetics of an SH3 domain to a PRM peptide, where a fluorinated tryptophan inserted in the SH3 domain allowed simultaneous monitoring of ^{19}F and $^1\text{H}/^{15}\text{N}$ chemical shift perturbations measured from the SH3 domain (Stadmler et al., 2020). The difference with our study is that the ^{19}F chemical shift perturbations report on the binding event from the point of view of the binding
435 | peptide, providing complementary information with the $^1\text{H}/^{15}\text{N}$ chemical shift perturbation from the SH3 domain. Here, observation of fluorine resonances perturbations on the ligand evidenced a different dynamics of the SH3 domain on the polyproline peptide upon introduction of the conformationally biased (4*S*)-FPro in the cognate PRM.

Although the available numerical tools allow in principle to model spin relaxation processes in multi-spin systems very accurately, a major complication is the picosecond scale dynamics of the five-membered ring, mainly due to the strong dependence of ^{19}F CSA on ring pucker. This effect can be mitigated by a strong ring pucker bias, as is typically the case for (4*R*)-
440 |

and (4*S*)-FPro residues. However, in general, and especially for other FPro variants without pucker bias (Hofman et al., 2018), a more advanced theoretical analysis will be required. Still, the measurement of the NOE between the geminal H γ and F γ provided an interesting way to probe local dynamics with correlation times between 0.3 and 4-5 ns.

445 The comparison of transverse relaxation at two different effective B₁ fields revealed the presence of motions occurring at the μ s to ms time-scale. It should be noted that the presence of many ¹H-¹⁹F couplings within the FPro spin system implies that recently developed ¹⁹F relaxation dispersion experiments cannot be applied (Overbeck et al., 2020). The dispersion of proton frequencies in the fluorinated prolines enable their selective excitation, a feature that was exploited for the selective H γ -F γ NOE and can be further used to develop sequences adapted to FPro spin systems. The molecular origin of the difference in dynamics between the oligoproline segments remains unclear, and suggests that the flanking amino acid sequences can play
450 a role in the conformational and dynamical preferences of polyproline segments. Importantly, given the absence of amide protons and the low ¹H α and ¹³C α chemical shift dispersion, this information would be very difficult to obtain from ¹H, ¹³C or ¹⁵N measurements.

In conclusion, fluorinated prolines provide an attractive tool for biomolecular NMR studies, in addition to their well-established application of controlling proline conformation. Given the increasing capabilities of chemical biology techniques
455 that allow introduction of unnatural amino acids in proteins, such as chemical ligation or genetic code expansion (Debelouchina et al., 2017), we foresee that ¹⁹F NMR studies through FPro residues will find their way to larger protein constructs. Apart from (4*R*)- and (4*S*)-fluorinated prolines, many more mono- and difluorinated prolines have been described (Verhoorck et al., 2018), providing a rich set of fluorine labelling options for PRMs that can be tuned to the specific needs in terms of conformational control and/or ¹⁹F NMR properties. Further investigations in this respect are ongoing. Furthermore,
460 this work demonstrates how the conformational changes caused by fluorination within a proline-rich SH3 binding motif subtly modulates the binding properties of an SH3 domain for its cognate binding site, despite it occurring at a position that is not directly involved in the binding – as defined by the canonical sequence binding motif – and the global PP-II conformation being preserved. We note that the change in binding affinity for the vinexin β SH3 upon (4*S*)-FPro insertion is comparable to what was observed upon serine phosphorylation in the proline-rich region of the RAR γ , upon which the MpRS and MpSR peptides were modelled upon (Lalevée et al. 2010). The introduction of fluoroproline in larger protein constructs
465 thus provides an attractive tool to explore how small local conformational biases result into large biological effects within interaction networks, which is the basis for signalling mechanisms. Indeed, binding sites for SH3 – or other – domains are frequently clustered within larger proline rich regions where post-translational modifications lead to subtle changes in the weak binding affinities and thus a redistribution of the protein-protein interaction network. We are confident that fluorinated
470 prolines and ¹⁹F NMR provide an elegant way to shed light on these complex systems.

5. Material and Methods

Sample preparation

475 The MpRS and MpSR peptides were produced by solid phase synthesis using Fmoc-amino-acids using a model 431A peptide synthesizer from Applied Biosystems (Foster City, CA, USA). Fmoc-protected (4*R*)- and (4*S*)-FPro amino acids were purchased from Bachem SA. Peptides were purified by reversed-phase HPLC, and checked by electrospray ionization-time of flight mass spectrometry (ESI-TOF). The Vinexin β SH3.3 was obtained using recombinant expression of a GST fusion protein in *E. coli* using pGEX plasmids as described (Lalevee et al., 2010). After thrombin cleavage, the protein was purified
480 using size exclusion chromatography and eluted with phosphate buffer (40 mM Phosphate, NaCl 100 mM, DTT 2 mM, pH 7). Before titration experiments, a dialysis was performed using 1 kDa and 3 kDa cutoff membrane for the peptide and the protein, respectively, and a common dialysis bath containing the buffer used in interactions experiments. Protein concentrations were determined by measuring the OD at 280 nm (molar absorption coefficient 11460 M⁻¹.cm⁻¹). Peptide concentrations were measured by ¹H NMR by comparing the integrals of peptide resonances with those of tryptophan of known concentration in a sample containing small amounts (10-30 μ M) of both compounds in D₂O as described (Kohler et al., 2015).
485 For assignments, lyophilized powder of MpRS and MpSR peptides were dissolved in 170 μ L of D₂O for a final concentration of 1 mM in 3 mm tubes.

NMR experiments

490 ¹⁹F NMR spectra were recorded on a Bruker Avance I spectrometer operating at a ¹H frequency of 600 MHz and equipped with a cryogenic QCI-F probe. ¹H and ¹³C spectra were recorded using a Bruker Avance III spectrometer operating at a ¹H frequency of 700 MHz and equipped with a cryogenic TCI probe. Standard full-range ¹H-¹³C HSQC (10 ppm ¹H x 80 ppm ¹³C) were recorded on MpRS and MpSR peptides for the carbon assignment. The number of points in the time domain was 4096 in *F*₂ and 4096 in *F*₁. In addition a high resolution 2D ¹H-¹³C HSQC-NOESY was recorded with the same ¹H spectral
495 width, but with a narrow carbon bandwidth of 3 ppm, centered on the proline's C δ resonances (47.3 ppm). The number of points in the time domain was 1024 in *F*₂ and 256 in *F*₁. The resulting resolution in the ¹³C dimension was 4 Hz/pt. The usual ¹³C 180° pulse used to compensate for chemical shift evolution during the *echo-antiecho* encoding pulsed field gradient was replaced by a frequency-selective ¹³C 180° refocusing pulse (4 ms RSNOB) was applied on the ¹³C δ region in order to avoid interference from folded peaks from outside the spectral region. The NOESY mixing time was 80 ms. The relaxation time was set to 1 s and 300 transients were recorded for each *t*₁ point resulting into a total experiment time of 1 day and
500 4 hours.

The ¹H-¹⁹F heteronuclear coupling constants were measured from the ¹H-¹H TOCSY spectra (MLEV spinlock 80 ms) recorded at 700 MHz. The spectral width was 10 ppm in both *F*₁ and *F*₂, with the number of time domain points 4096 in *F*₂ and 512 in *F*₁, resulting in resolutions in *F*₁ and *F*₂ of 23.4 and 2.9 Hz/pt, respectively. The ¹H-¹H couplings were measured using
505 SERF experiments (Fäcke et al., 1995) modified to use the Pell-Keeler method (Pell et al., 2007) to obtain 2D absorption mode line shapes, as recently proposed (Sinnaeve, 2021). The active spin refocussing selective 180° pulse was a RE-BURP pulse of 14.5 ms set to invert just the FPro H α signals, while the selective inversion 180° pulses were I-BURP pulses of 12.85 ms set to invert just one H β proton per FPro residue at a time. The spectral width was set to 1.07 ppm in *F*₂ and 23.5 Hz in *F*₁, with the number of time domain points 1024 in *F*₂ and 64 in *F*₁, resulting in resolutions in *F*₁ and *F*₂ of 0.7 and 1.5
510 Hz/pt, respectively.

¹⁹F R₁ and R₂ relaxation parameters were measured at 600 MHz (¹H frequency) and 298 K using standard inversion recovery and CPMG experiments respectively. The carrier frequency was set to -174 ppm with a spectral width of 12 ppm and an

interscan relaxation delay of 4 s. The inversion recovery relaxation build-up delays ranged from 1 ms to 3 s with an exponential sampling with one point repeated for uncertainty estimation, resulting in 20 data points in total. The CPMG sequence was measured using a half-echo delay of 200 μ s, or as a single spin echo with variable delays. A 180° proton pulse was applied every 2.8 ms at the fluorine echo time to average cross-correlation effects and ensure a single exponential decay (Farrow et al., 1995). Sampled relaxation delays ranged from 1 ms to 460 ms, with 16 data points in total.

¹H-¹⁹F nOe buildup experiments were measured by selectively saturating the H γ proton, using a train of sinc shaped soft 180° pulses centered at 5.42 ppm. The pulse duration was 2.8 ms and was applied every 4 ms prior to fluorine acquisition. The saturation times ranged from 10 ms to 2.6 s, including one repeat for error estimation, resulting in 16 data points in total. Processing of 1D ¹⁹F spectra and quantification were performed using an open-source Python package dedicated to Fourier spectroscopies called “Spectrometry Processing Innovative Kernel” (SPIKE) (Chiron et al., 2016). An exponential line broadening of 8 Hz was applied prior to Fourier Transform for signal apodization. Line fitting was done using the least-square minimizer of the Scipy optimize toolbox to find the optimal set of the signal parameters minimizing the squared differences between the experimental and calculated spectra. 2D spectra used for peptide assignments were processed using Topspin 2.6 (Bruker) and visualized in CcpNmr Analysis V2 (Vranken et al., 2005). Relaxation parameters were obtained by fitting relaxation data to a three parameters single exponential model using the least-square algorithm implemented in the Scipy optimize toolbox (Levenberg-Marquart).

The selective longitudinal relaxation rate constants ρ and the proton-fluorine cross-relaxation rate σ were obtained by identification of the three optimized parameters to the following equation:

$$I(t) = I_0 + \frac{\sigma \gamma_H}{\rho \gamma_F} I_0 (1 - e^{-\rho t}) \quad (3)$$

where I_0 is the equilibrium signal intensity and γ_H, γ_F are the proton and fluorine magnetogyric ratios, respectively.

Electronic structure theory and spin relaxation theory

All electronic structure theory calculations were performed using *Gaussian09* (Frisch et al., 2009). Molecular geometries of proline isomers and conformers were optimised for fluoroproline moieties (capped with an acetyl group on the NH side and a dimethylamino group on the COOH side) using density functional theory with the M06 exchange-correlation functional (Zhao et al., 2008) and cc-pVDZ basis set (Peterson et al., 2002) in SMD chloroform (Marenich et al., 2009). Hessians were checked for positive definiteness at convergence point, and magnetic property calculations (shielding tensors and J -couplings) then proceeded using gauge-independent atomic orbital method (London et al., 1937) with the basis set decontracted and augmented with tight Gaussian functions (Deng et al., 2006) for the calculation of isotropic J -couplings.

Spin relaxation theory calculations were performed using *Spinach 2.6* (Hogben et al., 2011). Cartesian coordinates, chemical shielding tensors, and J -couplings of all fluorine and hydrogen atoms were imported from *Gaussian09* logs, and a numerical evaluation (Goodwin et al., 2015) of Redfield’s relaxation superoperator (Redfield et al., 1957) for the resulting 16-spin system was carried out using the restricted state space approximation (Kuprov et al., 2007; Edwards et al., 2014), (IK-1(4,4) basis set) with a 5 Angstrom distance cut-off for dipolar interactions. Rigid-molecule isotropic rotational diffusion approximation was used. Longitudinal and transverse relaxation rates for the spins of interest were extracted as the matrix elements of the relaxation superoperator corresponding to L_z and L_+ states of those spins. The implementation of Bloch-Redfield-Wangsness theory in *Spinach* automatically accounts for all applicable cross-relaxation and cross-correlation effects (Kuprov et al., 2011).

Titration experiments

560 Titrations were performed by successive addition of stock peptide solutions to a sample of SH3 protein at 314 μM in a 3 mm NMR tube. In order to reduce the dilution of the initial protein solution and keep the aliquot volumes within values compatible with low pipetting errors (1 to 3 μL), initial aliquots were added using stock solutions diluted by a factor 2. The concentrations of the stock solutions were 5.1 mM and 5.7 mM for MpSR and MpRS, respectively. For every titration point, a 1D ^{19}F spectrum and a ^1H - ^{15}N -HSQC were recorded at 298K on the same spectrometer, taking advantage of the QCI-F probe. The ^1H - ^{15}N -HSQC was recorded using the standard pulse sequence and a 3-9-19 WATERGATE water suppression element. 565 200 points were recorded in the indirect dimension to achieve a final resolution of 7.0 and 18.8 Hz/pt in the acquisition and indirect dimensions, respectively. The relaxation delay was set to 1 s resulting in a total acquisition time of 16 min. The 1D ^{19}F spectra were recorded with a spectral width of 22522 kHz. The number of scans was adapted to achieve a sufficient signal/noise ratio for each concentration of peptide. For the first titration point, at a peptide concentration of 50 μM , 1600 scans were recorded for a total acquisition time of 1 hour and 6 min while 250 scans (10 min acquisition time) were used for the 570 large peptide concentrations. The protein chemical shift perturbation was averaged over 9 ^1H - ^{15}N correlations that displayed a similar apparent titration profile (from the amino-acids Q14, N15 (side chain $\text{N}_{\delta 2}$), D17, L21, W37 (side chain N_{ϵ}), V39, G49, T50, V56).

The composite chemical shift was calculated using:

575

$$\Delta\delta = \sqrt{(\Delta\delta_N)^2 + (5\Delta\delta_H)^2} \quad (4)$$

where $\Delta\delta_N$ and $\Delta\delta_H$ are the ^{15}N and proton chemical shift difference measured between the free protein and the protein in presence of a given amount of peptide.

580

The modeling of the interaction was performed using an in-house Python script that solves the equilibrium concentrations of a set of interacting molecules by integrating the set of coupled differential equations until steady state is reached (<https://github.com/delsuc/SpinEq>). To fit the experimental data, we used the fluorine frequencies of free and bound states, and the frequency of the bounded SH3 as parameters. Depending on the model, one or more equilibrium constants were 585 given. The goodness of fit was assessed using the reduced chi2:

$$\kappa^2 = \frac{1}{N-NP} \sum_{i=1}^N (\delta_i^{exp} - \delta_i^{calc})^2 \quad (5)$$

Acknowledgments

590

This work was supported by the Agence Nationale de la Recherche (FLUOVIAL ANR-18-CE44-0009-01, FLUOPROLINE ANR-20-CE11-0025) the French Infrastructure for Integrated Structural Biology (FRISBI, ANR-10-INSB-05-01), INSTRUCT-ERIC, the Centre National de la Recherche Scientifique and the University of Strasbourg. The Research Foundation – Flanders (FWO) is indebted for a research project to J.C.M. and D.S. (3G011015), a PhD fellowship to E.O. and staff exchange 595 funding (FWO-WOG Multimar). The EPSRC is thanked for a partial PhD grant to G.-J.H. (EPSRC-DTG EP/M50662X/1). A.B.B is supported by a fellowship from the région Grand Est and ANR. Claude Ling is warmly acknowledged for maintenance of the NMR spectrometers and Pascal Eberling for peptide synthesis.

600

6. References

- Ahuja P., Cantrelle F.X., Huvent I., Hanouille X., Lopez J., Smet C., Wieruszkeski J.M., Landrieu I., Lippens G.: Proline Conformation in a Functional Tau Fragment, *J. Mol. Biol.* 428 (2016) 79-91. <https://doi.org/10.1016/j.jmb.2015.11.023>
- 605 Aufiero, M., Gilmour, R.: Informing Molecular Design by Stereoelectronic Theory: The Fluorine Gauche Effect in Catalysis, *Acc. Chem. Res.* 51 (2018) 1701–1710. <https://doi.org/10.1021/acs.accounts.8b00192>.
- Behrendt, R. P., White, P., Offer, J.: Advances in Fmoc solid-phase peptide synthesis, *J. Pept. Sci.* 22 (2016) 4–27. <https://doi.org/10.1002/psc.2836>.
- 610 Berger, A. A., Völler, J.-S., Budisa, N., Kokschi, B.: Deciphering the Fluorine Code - The Many Hats Fluorine Wears in a Protein Environment, *Acc. Chem. Res.* 50 (2017) 2093–2103. <https://doi.org/10.1021/acs.accounts.7b00226>.
- Best, R. B., Merchant, K. A., Gopich, I. V., Schuler, B., Bax, A., Eaton W. A.: Effect of flexibility and cis residues in single-molecule FRET studies of polyproline, *Proc. Natl. Acad. Sci.* 104 (2007) 18964-18969. <https://doi.org/https://doi.org/10.1073/pnas.0709567104>.
- 615 Boeszoermerenyi, A., Chhabra, S., Dubey, A., Radeva, D. L., Burdzhiev, N. T., Chaney, C. D., Petrov, O. I., Gelev, V. M., Zhang, M., Anklin, C., Kovacs, H., Wagner, G., Kuprov, I., Takeuchi, K., Arthanari, H.: Aromatic ¹⁹F- ¹³C TROSY: a background-free approach to probe biomolecular structure, function, and dynamics, *Nat. Methods.* 16 (2019) 333–340. <https://doi.org/10.1038/s41592-019-0334-x>.
- Boeszoermerenyi, A., Ogórek, B., Jain, A., Arthanari, H., Wagner, G.: The precious fluorine on the ring: fluorine NMR for biological systems, *J. Biomol. NMR.* 74 (2020) 365–379. <https://doi.org/10.1007/s10858-020-00331-z>.
- 620 Bondi, A.: Van der waals volumes and radii, *J. Phys. Chem.* 68 (1964) 441–451. <https://doi.org/10.1021/j100785a001>.
- Borgogno, A., Ruzza, P.: The impact of either 4-R-hydroxyproline or 4-R-fluoroproline on the conformation and SH3m-cort binding of HPK1 proline-rich peptide, *Amino Acids.* 44 (2013) 607–614. <https://doi.org/10.1007/s00726-012-1383-y>.
- 630 Chaiken, I. M., Freedman, M. H., Lyerla, J. R., Cohen, J. S.: Preparation and studies of ¹⁹F-labeled and enriched ¹³C-labeled semisynthetic ribonuclease-S' analogues., *J. Biol. Chem.* 248 (1973) 884–891. [https://doi.org/10.1016/s0021-9258\(19\)44350-0](https://doi.org/10.1016/s0021-9258(19)44350-0).
- Chiron, L., Coutouly, M.-A., Starck, J.-P., Rolando, C., Delsuc, M.-A: SPIKE a Processing Software dedicated to Fourier Spectroscopies, (2016) 1–13. <http://arxiv.org/abs/1608.06777>.
- 635 Cordero, B., Gomez, V., Platero-Prats, A. E., Reves, M., Echeverria, J., Cremades, E., Barragan, F., Alvarez, S.: Covalent radii revisited, *J. Chem. Soc. Dalt. Trans.* (2008) 2832–2838. <https://doi.org/10.1039/b801115j>.
- Crowley, P. B., Kyne, C., Monteith, W. B.: Simple and inexpensive incorporation of ¹⁹F-Tryptophan for protein NMR spectroscopy, *Chem. Commun.* 48 (2012) 10681–10683. <https://doi.org/10.1039/c2cc35347d>.
- 640

- Dalvit, C., Piotto, M.: ^{19}F NMR transverse and longitudinal relaxation filter experiments for screening: a theoretical and experimental analysis, *Magn. Reson. Chem.* 55 (2017) 106–114. <https://doi.org/10.1002/mrc.4500>.
- Debelouchina, G. T., Muir, T. W.: A molecular engineering toolbox for the structural biologist, *Q. Rev. Biophys.* 50 (2017). <https://doi.org/10.1017/S0033583517000051>.
- 645 Deng, W., Cheeseman, J. R., Frisch, M. J.: Calculation of nuclear spin-spin coupling constants of molecules with first and second row atoms in study of basis set dependence, *J. Chem. Theory Comput.* 2 (2006) 1028–1037. <https://doi.org/10.1021/ct600110u>.
- DeRider, M. L., Wilkens, S. J., Waddell, M. J., Bretscher, L. E., Weinhold, F., Raines, R. T., Markley, J. L.: Collagen stability: Insights from NMR spectroscopic and hybrid density functional computational investigations of the effect of
650 electronegative substituents on prolyl ring conformations, *J. Am. Chem. Soc.* 124 (2002) 2497–2505. <https://doi.org/10.1021/ja0166904>.
- Dietz D., Kubyskhin V., Budisa N.: Applying gamma-Substituted Prolines in the Foldon Peptide: Polarity Contradicts Pre-organization, *Chembiochem* 16 (2015) 403-406. <https://doi.org/10.1002/cbic.201402654>.
- 655 Eberhardt, E. S., Panasik, N., Raines, R. T.: Inductive effects on the energetics of prolyl peptide bond isomerization: Implications for collagen folding and stability, *J. Am. Chem. Soc.* 118 (1996) 12261–12266. <https://doi.org/10.1021/ja9623119>.
- Edwards, L. J., Savostyanov, D. V., Welderufael, Z. T., Lee, D., Kuprov, I.: Quantum mechanical NMR simulation algorithm for protein-size spin systems, *J. Magn. Reson.* 243 (2014) 107–113. <https://doi.org/10.1016/j.jmr.2014.04.002>.
- 660 Eftekhazadeh, B., Piai, A., Chiesa, G., Mungianu, D., Garcia, J., Pierattelli, R., Felli, I.C., Salvatella X.: Sequence Context Influences the Structure and Aggregation Behavior of a PolyQ Tract, *Biophysical Journal* 110 (2016) 2361-2366. <https://doi.org/10.1016/j.bpj.2016.04.022>
- Evanics, F., Bezsonova, I., Marsh, J., Kitevski, J. L., Forman-Kay, J. D., Prosser, R.S.: Tryptophan Solvent Exposure in Fold-
665 ed and Unfolded States of an SH3 Domain by ^{19}F and ^1H NMR, *Biochemistry.* 129 (2007) 1826–1835. <https://doi.org/10.1021/bi061389r>
- Fäcke, T., Berger, S.: SERF, a New Method for ^1H , ^1H Spin-Coupling Measurement in Organic Chemistry, *J. Magn. Reson. Ser. A.* 113 (1995) 114–116. <https://doi.org/10.1006/jmra.1995.1063>.
- Farrow, N. A., Zhang, O., Forman-Kay, J.D., Kay, L.E.: Comparison of the Backbone Dynamics of a Folded and an Unfold-
670 ed SH3 Domain Existing in Equilibrium in Aqueous Buffer, *Biochemistry.* 34 (1995) 868–878. <https://doi.org/10.1021/bi00003a021>.
- Ferreiro, D. U., Komives, E. A., Wolynes, P. G.: Frustration in biomolecules, *Q. Rev. Biophys.* 47 (2014) 285–363. <https://doi.org/10.1017/S0033583514000092>.

- 675 Frisch, M.J., Trucks, G.W., Schlegel, H.B., Scuseria, G.E., Robb, M.A., Cheeseman, J.R., Scalmani, G., Barone, V., Men-
nucci, B., Petersson, G.A., Nakatsuji, H., Caricato, M., Li, X., Hratchian, H.P., Izmaylov, A.F., Bloino, J., Zheng,
G., Sonnenberg, J.L., Hada, M., Ehara, M., Toyota, K., Fukuda, R., Hasegawa, J., Ishida, M., Nakajima, T., Honda,
Y., Kitao, O., Nakai, H., Vreven, T., Montgomery, J.A., Jr., Peralta, J.E., Ogliaro, F., Bearpark, M., Heyd, J.J.,
Brothers, E., Kudin, K.N., Staroverov, V.N., Kobayashi, R., Normand, J., Raghavachari, K., Rendell, A., Burant,
680 J.C., Iyengar, S.S., Tomasi, J., Cossi, M., Rega, N., Millam, N.J., Klene, M., Knox, J.E., Cross, J.B., Bakken, V.,
Adamo, C., Jaramillo, J., Gomperts, R., Stratmann, R.E., Yazyev, O., Austin, A. J., Cammi, R., Pomelli, C., Ochter-
ski, J. W., Martin, R.L., Morokuma, K., Zakrzewski, V.G., Voth, G.A., Salvador, P., Dannenberg, J.J., Dapprich, S.,
Daniels, A.D., Farkas, Ö., Foresman, J.B., Ortiz, J.V., Cioslowski, J., Fox, D.J. Gaussian 09, in, Gaussian, Inc., Wall-
ingford CT, USA, 2009.
- Gee, C. T., Arntson, K. E., Urick, A. K., Mishra, N. K., Hawk, L. M. L., Wisniewski, A. J., Pomerantz, W. C. K.: Protein-
685 observed ¹⁹F-NMR for fragment screening, affinity quantification and druggability assessment, Nat. Protoc. 11 (2016) 1414–
1427. <https://doi.org/10.1038/nprot.2016.079>
- Gerig, J., McLeod, R.: Conformations of cis- and trans-4-Fluoroproline in Aqueous Solution, J. Am. Chem. Soc. 17 (1973)
4788–4795. <https://doi.org/10.1021/ja00798a046>.
- Gillis, E. P., Eastman, K. J., Hill, M. D., Donnelly, D. J., Meanwell, N. A.: Applications of Fluorine in Medicinal Chemistry,
690 J. Med. Chem. 58 (2015) 8315–8359. <https://doi.org/10.1021/acs.jmedchem.5b00258>.
- Gimenez, D., Phelan, A., Murphy, C. D., Cobb S. L.: ¹⁹F NMR as a tool in chemical biology, J. Org. Chem. 17 (2021) 293–
318. <https://doi.org/10.3762/BJOC.17.28>.
- Goodwin, D. L., Kuprov, I.: Auxiliary matrix formalism for interaction representation transformations, optimal control, and
spin relaxation theories, J. Chem. Phys. 143 (2015). <https://doi.org/10.1063/1.4928978>.
- 695 Hofman, G.-J., Ottoy, E., Light, M., Kieffer, B., Kuprov, I., Martins, J. C., Sinnaeve, D., Linclau, B.: Minimising conforma-
tional bias in fluoroprolines through vicinal difluorination, Chem. Commun. 54 (2018) 5118–5121.
<https://doi.org/10.1039/c8cc01493k>.
- Hofman, G.-J., Ottoy, E., Light, M. E., Kieffer, B., Martins, J. C., Kuprov, I., Sinnaeve, D., Linclau, B.: Synthesis and Con-
formational Properties of 3,4-Difluoro-1-prolines, J. Org. Chem. 84 (2019) 3100–3120.
700 <https://doi.org/10.1021/acs.joc.8b02920>.
- Hogben, H. J., Krzystyniak, M., Charnock, G. T. P., Hore, P. J., Kuprov, I.: Spinach - A software library for simulation of
spin dynamics in large spin systems, J. Magn. Reson. 208 (2011) 179–194.
<https://doi.org/10.1016/j.jmr.2010.11.008>.
- Holmgren, S. K., Taylor, K. M., Bretscher, L. E., Raines, R. T.: Code for Collagen's Stability Deciphered, Nature. 392
705 (1998) 666–667. <https://doi.org/10.1038/33573>.
- Hornig, J.-C. Raines, R.T.: Stereoelectronic effects on polyproline conformation, Protein Sci. 15 (2006) 74–83.
<https://doi.org/10.1110/ps.051779806>.

- Jiji, A. C., Shine, A., Vijayan, V.: Direct Observation of Aggregation-Induced Backbone Conformational Changes in Tau Peptides, *Angew. Chemie - Int. Ed.* 55 (2016) 11562–11566. <https://doi.org/10.1002/anie.201606544>.
- 710 Kang, Y. K.: Puckering transition of proline residue in water, *J. Phys. Chem. B.* 111 (2007) 10550–10556. <https://doi.org/10.1021/jp073411b>.
- Kim, T. H., Mehrabi, P., Ren, Z., Sljoka, A., Ing, C., Bezginov, A., Ye, L., Pomès, R., Prosser, R. S., Pai, E. F.: The role of dimer asymmetry and protomer dynamics in enzyme catalysis, *Science.* 355 (2017) 6-11. <https://doi.org/10.1126/science.aag2355>.
- 715 Kitevski-LeBlanc, J. L., Prosser, R. S.: Current applications of ^{19}F NMR to studies of protein structure and dynamics, *Prog. Nucl. Magn. Reson. Spectrosc.* 62 (2012) 1–33. <https://doi.org/10.1016/j.pnmrs.2011.06.003>.
- Kohler, C., Recht, R., Quinternet, M., de Lamotte, F., Delsuc, M.-A., Kieffer, B.: Accurate Protein–Peptide Titration Experiments by Nuclear Magnetic Resonance Using Low-Volume Samples, *Methods Mol. Biol.* 1286 (2015) 279–296. https://doi.org/10.1007/978-1-4939-2447-9_22.
- 720 Kovrigin, E. L.: NMR line shapes and multi-state binding equilibria, *J. Biomol. NMR.* 53 (2012) 257–270. <https://doi.org/10.1007/s10858-012-9636-3>.
- Kubyshev, V., Davis, R., Budisa, N.: Biochemistry of fluoroproline: The prospect of making fluorine a bioelement, *J. Org. Chem.* 17 (2021) 439–450. <https://doi.org/10.3762/BJOC.17.40>.
- Kuprov, I., Wagner-Rundell, N., Hore, P.J.: Polynomially scaling spin dynamics simulation algorithm based on adaptive state-space restriction, *J. Magn. Reson.* 189 (2007) 241–250. <https://doi.org/10.1016/j.jmr.2007.09.014>.
- 725 Kuprov, I.: Diagonalization-free implementation of spin relaxation theory for large spin systems, *J. Magn. Reson.* 209 (2011) 31–38. <https://doi.org/10.1016/j.jmr.2010.12.004>.
- Lalève, S., Bour, G., Quinternet, M., Samarut, E., Kessler, P., Vitorino, M., Bruck, N., Delsuc, M.-A., Vonesch, J.-L., Kieffer, B., Rochette-Egly, C.: Vinexin β , an atypical “sensor” of retinoic acid receptor γ signaling: union and sequestration, separation, and phosphorylation, *FASEB J.* 24 (2010) 4523–4534. <https://doi.org/10.1096/fj.10-160572>.
- 730 Liu, J. J., Horst, R., Katritch, V., Stevens, R. C., Wüthrich, K.: Biased signaling pathways in β 2-adrenergic receptor characterized by ^{19}F -NMR, *Science.* 335 (2012) 1106–1110. <https://doi.org/10.1126/science.1215802>.
- London, F.: Théorie quantique des courants interatomiques dans les combinaisons aromatiques, *J. Phys. Le Radium.* 8 (1937) 397–409. <https://doi.org/10.1051/jphysrad:01937008010039700>.
- 735 London, R. E.: On the Interpretation of ^{13}C Spin-Lattice Relaxation Resulting from Ring Puckering in Proline, *J. Am. Chem. Soc.* 100 (1978) 2678–2685. <https://doi.org/10.1021/ja00477a018>.
- Lu, M., Ishima, R., Polenova, T., Gronenborn, A.M.: ^{19}F NMR relaxation studies of fluorosubstituted tryptophans, *J. Biomol. NMR.* 73 (2019) 401–409. <https://doi.org/10.1007/s10858-019-00268-y>.

- Marenich, A. V., Cramer, C. J., Truhlar, D. G.: Universal solvation model based on solute electron density and on a continuum model of the solvent defined by the bulk dielectric constant and atomic surface tensions, *J. Phys. Chem. B.* 113 (2009) 6378–6396. <https://doi.org/10.1021/jp810292n>.
- Mei, H., Han, J., Klika, K. D., Izawa, K., Sato, T., Meanwell, N. A., Soloshonok V. A.: Applications of fluorine-containing amino acids for drug design, *Eur. J. Med. Chem.* 186 (2020) 111826. <https://doi.org/10.1016/j.ejmech.2019.111826>.
- Muttenthaler, M., King, G. F., Adams, D.J., Alewood, P. F.: Trends in peptide drug discovery, *Nat. Rev. Drug Discov.* 20 (2021) 309–325. <https://doi.org/10.1038/s41573-020-00135-8>.
- Newberry, R. W., Raines, R. T.: 4-Fluoroprolines: Conformational Analysis and Effects on the Stability and Folding of Peptides and Proteins, *Topics in Heterocyclic Chemistry: Peptidomimetics I.* (2016) 1–11. https://doi.org/10.1007/7081_2015_196.
- Odar, C., Winkler, M., Wiltschi, B.: Fluoro amino acids: A rarity in nature, yet a prospect for protein engineering, *Biotechnol. J.* 10 (2015) 427–446. <https://doi.org/10.1002/biot.201400587>.
- O'Hagan, D.: Understanding organofluorine chemistry. An introduction to the C–F bond, *Chem. Soc. Rev.* 37 (2008) 308–319. <https://doi.org/10.1039/b711844a>.
- O'Hagan, D.: Organofluorine chemistry: Synthesis and conformation of vicinal fluoromethylene motifs, *J. Org. Chem.* 77 (2012) 3689–3699. <https://doi.org/10.1021/jo300044q>.
- Overbeck, J.H., Kremer, W., Sprangers, R.: A suite of ¹⁹F based relaxation dispersion experiments to assess biomolecular motions, *J. Biomol. NMR.* 74 (2020) 753–766. <https://doi.org/10.1007/s10858-020-00348-4>.
- Panasik, N., Eberhardt, E. S., Edison, A. S., Powell, D. R., Raines, R. T.: Inductive effects on the structure of proline residues, *Int. J. Pept. Protein Res.* 44 (1994) 262–269. <https://doi.org/10.1111/j.1399-3011.1994.tb00169.x>.
- Pell, A. J., Keeler, J.: Two-dimensional J-spectra with absorption-mode lineshapes, *J. Magn. Reson.* 189 (2007) 293–299. <https://doi.org/10.1016/j.jmr.2007.09.002>.
- Peterson, K. A., Dunning, T. H.: Accurate correlation consistent basis sets for molecular core-valence correlation effects: The second row atoms Al–Ar, and the first row atoms B–Ne revisited, *J. Chem. Phys.* 117 (2002) 10548–10560. <https://doi.org/10.1063/1.1520138>.
- Rastinejad, F., Evilia, C., Lu, P.: Studies of Nucleic Acids and Their Protein Interactions by ¹⁹F NMR, *Methods Enzymol.*, 261 (1995) 560–575. [https://doi.org/10.1016/s0076-6879\(95\)61025-1](https://doi.org/10.1016/s0076-6879(95)61025-1).
- Redfield, A.G.: On the Theory of Relaxation Processes, *IBM J. Res. Dev.* (1957) 19–31. <https://doi.org/10.1147/rd.11.0019>.
- Ruzza, P., Siligardi, G., Donella-Deana, A., Calderan, A., Hussain, R., Rubini, C., Cesaro, L., Osler, A., Guiotto, A., Pinna, L. A., Borin, G. 4-Fluoroproline derivative peptides: Effect on PPII conformation and SH3 affinity, *J. Pept. Sci.* 12 (2006) 462–471. <https://doi.org/10.1002/psc.750>.

- Salwiczek, M., Nyakatura, E. K., Gerling, U. I. M., Ye, S., Kokschi, B.: Fluorinated amino acids: Compatibility with native protein structures and effects on protein–protein interactions, *Chem. Soc. Rev.* 41 (2012) 2135–2171.
<https://doi.org/10.1039/c1cs15241f>.
- 775 Saksela, K., Permi, P.: SH3 domain ligand binding: What’s the consensus and where’s the specificity?, *FEBS Lett.* 586 (2012) 2609–2614. <https://doi.org/10.1016/j.febslet.2012.04.042>.
- Sarkar, S. K., Young, P. E., Torchia, D. A.: Ring Dynamics of DL-Proline and DL-Proline Hydrochloride in the Solid State: A ^2H Nuclear Magnetic Resonance Study, *J. Am. Chem. Soc.* 108 (1986) 6459–6464.
<https://doi.org/10.1021/ja00281a002>.
- 780 Sharaf, N. G., Gronenborn, A. M.: ^{19}F -Modified Proteins and ^{19}F -Containing Ligands as Tools in Solution NMR Studies of Protein Interactions, *Methods Enzymol.* 565 (2015) 67–95. <https://doi.org/10.1016/bs.mie.2015.05.014>.
- Sinnaeve, D. Selective Homonuclear 2D J-Resolved Spectroscopy. *eMagRes* 9 (2021) 267–282.
<https://doi.org/10.1002/9780470034590.emrstm1544>
- Schubert, M., Labudde, D., Oschkinat, H., Schmieder, P.: A software tool for the prediction of Xaa-Pro peptide bond conformations in proteins based on ^{13}C chemical shift statistics, *J. Biomol. NMR.* 24 (2002) 149–154.
785 <https://doi.org/10.1023/A:1020997118364>.
- Shoulders, M.D., Raines, R.T.: Collagen structure and stability, *Annu. Rev. Biochem.* 78 (2009) 929–958.
<https://doi.org/10.1146/annurev.biochem.77.032207.120833>.
- Stadmler, S.S., Aguilar, J.S., Waudby, C.A., Pielak, G.J.: Rapid Quantification of Protein-Ligand Binding via ^{19}F NMR Lineshape Analysis, *Biophys. J.* 118 (2020) 2537–2548. <https://doi.org/10.1016/j.bpj.2020.03.031>.
- 790 Theillet, F.-X., Kalmar, L., Tompa, P., Han, K.-H., Selenko, P., Dunker, A. K., Daughdrill, G. W., Uversky, V. N.: The alphabet of intrinsic disorder, *Intrinsically Disord. Proteins.* 1 (2013) e24360. <https://doi.org/10.4161/idp.24360>.
- Thiehoff, C., Rey, Y.P., Gilmour, R.: The Fluorine Gauche Effect: A Brief History, *Isr. J. Chem.* 57 (2017) 92–100.
<https://doi.org/10.1002/ijch.201600038>.
- Torbeev, V., Ebert, M. O., Dolenc, J., Hilvert, D.: Substitution of proline³² by α -methylproline preorganizes β 2-microglobulin for oligomerization but not for aggregation into amyloids, *J. Am. Chem. Soc.* 137 (2015) 2524–2535.
795 <https://doi.org/10.1021/ja510109p>.
- Torbeev, V.Y., Hilvert, D.: Both the cis-trans equilibrium and isomerization dynamics of a single proline amide modulate β 2-microglobulin amyloid assembly, *Proc. Natl. Acad. Sci. U. S. A.* 110 (2013) 20051–20056.
<https://doi.org/10.1073/pnas.1310414110>.
- 800 Urbanek, A., Popovic, M., Elena-Real, C. A., Morató, A., Estaña, A., Fournet, A., Allemand, F., Gil, A. M., Cativiela, C., Cortés, J., Jiménez, A. I., Sibille, N., Bernadó, P.: Evidence of the Reduced Abundance of Proline cis Conformation in Protein Poly Proline Tracts, *J. Am. Chem. Soc.* 142 (2020) 7976–7986. <https://doi.org/10.1021/jacs.0c02263>.

- Urbanek, A., Popovic, M., Morató, A., Estaña, A., Elena-Real, C.A., Mier, P., Fournet, A., Allemand, F., Delbecq, S., Andrade-Navarro, M.A., Cortés, J., Sibille, N., Bernadó, P.: Flanking regions determine the structure of the polyglutamine in huntingtin through mechanisms common among glutamine-rich human proteins, *Structure* 28 (2020) 733-746 <https://doi.org/10.1016/j.str.2020.04.008>
- 805
- Verhoorck, S. J. M., Killoran, P. M., Coxon, C. R.: Fluorinated Prolines as Conformational Tools and Reporters for Peptide and Protein Chemistry, *Biochemistry* 57 (2018) 6132–6143. <https://doi.org/10.1021/acs.biochem.8b00787>.
- 810
- Vranken, W. F., Boucher, W., Stevens, T. J., Fogh, R. H., Pajon, A., Llinas, M., Ulrich, E. L., Markley, J. L., Ionides, J., Laue, E. D.: The CCPN data model for NMR spectroscopy: Development of a software pipeline, *Proteins Struct. Funct. Genet.* 59 (2005) 687–696. <https://doi.org/10.1002/prot.20449>.
- Welte, H., Zhou, T., Mihajlenko, X., Mayans, O., Kovermann, M.: What does fluorine do to a protein? Thermodynamic, and highly-resolved structural insights into fluorine-labelled variants of the cold shock protein, *Sci. Rep.* 10 (2020) 1–12. <https://doi.org/10.1038/s41598-020-59446-w>.
- 815
- Wilhelm, P., Lewandowski, B., Trapp, N., Wennemers, H.: A crystal structure of an oligoproline PPII-Helix, at last, *J. Am. Chem. Soc.* 136 (2014) 15829–15832. <https://doi.org/10.1021/ja507405j>.
- Yoshida, A.: Studies on the mechanism of protein synthesis, Incorporation of p-fluorophenylalanine into α -amylase of *Bacillus subtilis*, *BBA - Biochim. Biophys. Acta.* 41 (1960) 98–103. [https://doi.org/10.1016/0006-3002\(60\)90373-5](https://doi.org/10.1016/0006-3002(60)90373-5)
- 820
- Zhao, Y., Truhlar, D.G.: The M06 suite of density functionals for main group thermochemistry, thermochemical kinetics, noncovalent interactions, excited states, and transition elements: Two new functionals and systematic testing of four M06-class functionals and 12 other functionals, *Theor. Chem. Acc.* 120 (2008) 215–241. <https://doi.org/10.1007/s00214-007-0310-x>.
- 825
- Zhang, C., Moonshi, S. S., Han, Y., Puttick, S., Peng, H., Magoling, B. J. A., Reid, J. C., Bernardi, S., Searles, D. J., Král, P., Whittaker, A. K.: PFPE-Based Polymeric ^{19}F MRI Agents: A New Class of Contrast Agents with Outstanding Sensitivity, *Macromolecules.* 50 (2017) 5953–5963. <https://doi.org/10.1021/acs.macromol.7b01285>.

830